THE FUNDAMENTAL SOLUTION OF THE TIME-DEPENDENT SYSTEM OF CRYSTAL OPTICS

By

Robert Burridge

and

Jianliang Qian

IMA Preprint Series # 2083

(December 2005)

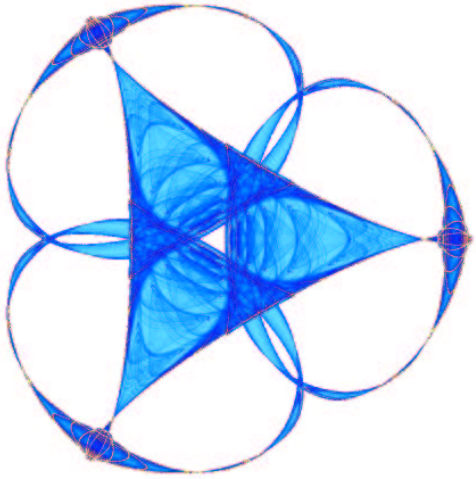

INSTITUTE FOR MATHEMATICS AND ITS APPLICATIONS

UNIVERSITY OF MINNESOTA

400 Lind Hall

207 Church Street S.E.

Minneapolis, Minnesota 55455–0436

Phone: 612/624-6066 Fax: 612/626-7370

URL: http://www.ima.umn.edu

The Fundamental Solution of the Time-Dependent System of Crystal Optics

Robert Burridge * Jianliang Qian†

November 22, 2005

Abstract

We set up the electromagnetic system and its plane-wave solutions with the associated slowness and wave surfaces. We treat the Cauchy initial-value problem for the electric vector and make explicit the quantities necessary for numerical evaluation. We use the Herglotz-Petrovskii representation as an integral around loops which, for each position and time form the intersection of a plane in the space of slownesses with the slowness surface. The field and especially its singularities are strongly dependent on the varying geometry of these loops; we use a level set numerical technique to compute those real loops which essentially give us second order accuracy. We give the static term corresponding to the mode with zero wave speed. Numerical evaluation of the solution is presented graphically followed by some concluding remarks.

Key Words: crystal optics, conical refraction, Maxwell's equation, fundamental solution

1 Introduction

1.1 General introduction

Crystal optics is similar to, but simpler than, anisotropic elasticity. For instance its slowness surface has conical points, in common with many elasticity systems, and there are conical points on the wave surface. It also has a third interesting feature associated with the role of the divergence in relation to Maxwell's equations, namely the fact that one characteristic speed is zero (actually two coincident zeros), so that the slowness surface is quartic rather than sextic as might be expected from the dimensionality - one quadratic sheet of the slowness surface lies at infinity. Remarkably the wave surface is another quartic surface of the same

*Earth Resources Laboratory, Massachusetts Institute of Technology, 42 Carleton Street, E34-450, Cambridge, MA 02142-1324. Email: **burridge@erl.mit.edu**

†Department of Mathematics and Statistics, Wichita State University, Wichita, KS 67260-0033. Email: **qian@math.wichita.edu**. This author is supported by NSF DMS-0542174.

algebraic type, but with reciprocal parameters. See for instance Born and Wolf (1989) for a very full and readable account of the plane-wave theory of this system and the associated geometry.

The system of crystal optics is of great intrinsic and historical interest, the latter because Hamilton's prediction in 1833 of internal conical refraction, and Lloyd's experimental confirmation closely thereafter, led to the wide acceptance of Fresnel's wave theory of light. The intrinsic interest is largely centered around the remarkable geometrical properties of the slowness surface and wave surface, which are both of a type known as Fresnel's wave surface (Salmon, 1915).

We derive the fundamental solution for the time-dependent system of crystal optics in the space-time domain. Furthermore, we illustrate numerically the analytic expression for the fundamental solution of the system in terms of real loop integrals according to the Herglotz-Petrovskii formula, which may also be applied readily to other constant-coefficient hyperbolic systems. Petrovskii (1945) expressed the solution in terms of non-real cycles in complex space. Atiyah, Bott, and Garding (1970, 1973) placed Petrovskii's work on a modern basis, and Smit and De Hoop (1995) recently elaborated this in a three-dimensional elastodynamic setting. But following John (1955) and Gelfand and Shilov (1964) we will stay with the representation in terms of real integrals. Burridge (1967) used it to obtain the geometrical arrivals (see below), and the singularity due to the conical points of the slowness surface at field points in the interior of the cone of internal conical refraction for cubic elastic media. But that work lacked numerical illustrations and the treatment of the conical point was not uniform near the conical surface itself. Although we still do not give the uniform time-dependent asymptotic analysis for this region, we do present numerical solutions close to and on this 'cone of internal conical refraction'. The geometrical arrivals mentioned above are singularities in the field associated with slownesses $\boldsymbol{\xi}$ which are 'stationary points' where the plane $\boldsymbol{\xi}\cdot\boldsymbol{x} = t$ touches the slowness surface and at which the slowness surface has finite non-zero Gaussian curvature, and such wave arrivals are governed by the simplest form of geometrical ray theory.

For instance Moskvin et al. (1993) have derived the Green's function in the frequency domain and discussed various important directions and cones of directions in relation to the field, namely in the directions of generators of the cone of internal conical refraction, and in the directions of the bi-radials, i.e. the directions of the conical points on the wave surface, and they obtain asymptotic approximations to the field at large distances in the neighborhoods of these directions. Based on Moskvin et al. (1993), Warnick and Arnold (1997) made further detailed studies of the conical refraction. Recently, Berry (2004) applied the paraxial optics to study this singularity; his findings have extended and complemented the existing theory by providing detailed analysis of such singularity. All of the above cited works for the internal conical refraction are based on the space-frequency formulation.

In this paper we study the second-order vector equation for $\boldsymbol{E}$ obtained by eliminating the other dependent variables from Maxwell's equations and the constitutive laws of crystal optics. This equation is like the second-order elastodynamic equation for particle displacement and may be obtained from that of isotropic infinitesimal elasticity by setting the Lamé constant $\lambda = -2$, and $\mu = 1$, so that $\lambda + 2\mu = 0$, and the density $\rho = \boldsymbol{\sigma}$ (see below).

Crystals fall under three symmetry classes which affect the optical properties. Either three eigenvalues of the dielectric tensor are all distinct (bi-axial crystal), or two eigenvalues are equal but unequal to the third (uni-axial crystal), or all three eigenvalues are equal (optically isotropic crystal). In this paper we shall concentrate on the bi-axial case.

Our approach is based on the space-time formulation which can be used to further study the internal conical refraction; the numerical analysis carried out in the current work complements the earlier mathematical investigations done by Ludwig (1961), Melrose and Uhlmann (1979) and Uhlmann (1982). In particular, with modern microlocal analysis tools Melrose and Uhlmann (1979) have constructed the microlocal parametrix for the Cauchy problem of Maxwell's equation in a bi-axial crystal to analyze the singularities of the solution so that they were able to explain the appearance of the cone of conical refraction when a ray of light hits a bi-axial crystal in a direction parallel to an optic axis of the crystal. Furthermore, based on Melrose and Uhlmann (1979), Uhlmann (1982) carried out a more elegant and refined analysis than the study of the singularities to explain the so-called "double ring" phenomena; see Uhlmann (1982) for more details.

On the other hand, Taylor and Uhlmann (Taylor, 1981; Chapter 15, Section 5) have constructed a microlocal parametrix to deal with the phenomenon of conical refraction. They first perturbed the second order equation for the electric vector so that the equation behaves like an elastic system; then they defined the so-called conical singularity via the characteristic variety and the conic variety. Here we notice that the characteristic variety in their setting is equivalent to the slowness surface in our setting. In particular, they constructed the fundamental solution at a conical singular point, and it is represented as a tensor product between a δ-function and the distributional kernel of the classical wave equation in three variables.

However, in this work we construct the fundamental solution for the second order equation for the electric vector in the whole space, hence it is different from the one constructed by Taylor and Uhlmann. On the other hand, the numerical computation of the fundamental solution of the Cauchy problem presented here does illustrate related singularities in the field associated with slownesses $\boldsymbol{\xi}$ which are 'stationary points' where the plane $\boldsymbol{\xi}\cdot\boldsymbol{x} = t$ touches the slowness surface and at which the slowness surface has finite non-zero Gaussian curvature (see below). See Every (1981) for the effects of curvature of the slowness surface near crystal symmetry axes in cubic crystal acoustics, Shuvalov and Every (1996) for more general symmetries, and Musgrave (1970) for the general theory of crystal acoustics.

In this work we concentrate on the fundamental solution for the constant-coefficient time-dependent non-dispersive system of crystal optics in the space-time formulation. For the variable-coefficient time-dependent system of crystal optics in the space-time domain, Braam and Duistermaat (1993) predict singularities that spiral or glance hyperbolically in the vicinity of the so-called "double characteristic set", and the derivatives of the material properties are responsible for such singularities. To deal with such a case, we may start from normal forms of real symmetric systems with multiplicity developed in Braam and Duistermaat (1993) and go along the lines developed in Burridge (1967) to study singularities related to the internal conical refraction of light; the related numerical investigation is an ongoing work.

1.2 Outline of this paper

In Section 2 we set up the electromagnetic system and its plane-wave solutions with the associated geometrical entities such as the slowness surface, and the wave surface. In Section 3 we set up and solve the Cauchy initial-value problem for $\boldsymbol{E}$ and make explicit some quantities with a view to numerical evaluation. In Section 4 we follow the Herglotz-Petrovskii procedure of transforming the integral representation to an integral around loops which, for each $\boldsymbol{x}, t$, form the intersection of the plane $\boldsymbol{\xi}\cdot\boldsymbol{x} = t$ with the slowness surface. As $\boldsymbol{x}, t$ vary the geometry of these loops varies; the field and especially its singularities are strongly dependent on the geometry of these loops. In Section 5 we give the static term corresponding to the mode with zero wave speed. Numerical evaluation of the fundamental solution is presented graphically in Section 6 for a selection of points in the positive quadrant of the 13-plane. Section 7 contains some concluding remarks.

Table of notations:

Symbol	Definition
$t.$	time
$\boldsymbol{x} = (x_1, x_2, x_3)$	spatial coordinate vector.
$\boldsymbol{r} = (r_1, r_2, r_3)$	coordinate vector for the representation of $\mathcal{E}$.
c	the speed of light *in vacuo*.
$\boldsymbol{E}$, $\boldsymbol{H}$	the electric and magnetic vectors.
$\boldsymbol{D}$	The electric displacement.
$\boldsymbol{B}$	The magnetic induction.
μ	The magnetic permeability (scalar).
$\boldsymbol{\epsilon}$	The dielectric tensor (symmetric).
$\boldsymbol{\sigma}$, σ_1, σ_2, σ_3	$\mu\boldsymbol{\epsilon}/c^2$ and its principal values.
$\boldsymbol{\xi}$	The slowness vector.
f	Plane wave pulse shape.
$\boldsymbol{e}$, $\boldsymbol{h}$, $\boldsymbol{d}$, $\boldsymbol{b}$	Constant polarization vectors for $\boldsymbol{E}$, $\boldsymbol{H}$, $\boldsymbol{D}$, $\boldsymbol{B}$, related to $\boldsymbol{\xi}$.
$\hat{\boldsymbol{x}}$	The unit vector in the direction of $\boldsymbol{x}$, and similarly for other vectors.
$\hat{\boldsymbol{x}}$, $\hat{\boldsymbol{y}}$, $\hat{\boldsymbol{z}}$, $\boldsymbol{x}^\perp$	Unit vectors (Section 5 and Appendix A only).
Ω, $\mathrm{d}\Omega$	The unit sphere and its surface element.
$\mathcal{E}$	The energy ellipsoid $\boldsymbol{r}^T\boldsymbol{\sigma}^{-1}\boldsymbol{r} = 1$.
u, v	Ellipsoidal coordinates on ellipsoid $\mathcal{E}$ $(\sigma_1 \geq u \geq \sigma_2 \geq v \geq \sigma_3 \geq 0.)$
$\mathcal{S}$, $\mathrm{d}S$	The slowness surface and its surface element.
$\boldsymbol{c}_\mathcal{S}$	A conical point on $\mathcal{S}$.
$\Pi_\mathcal{S}$	One of the four special tangent planes to $\mathcal{S}$.
$\mathcal{C}_\mathcal{S}$	One of the four circles in which a $\Pi_\mathcal{S}$ touches $\mathcal{S}$.
$\mathcal{W}$	The wave surface (reciprocal to $\mathcal{S}$).

Symbol	Definition
$\boldsymbol{c}_{\mathcal{W}}$	A conical point on $\mathcal{W}$ (reciprocal to $\Pi_{\mathcal{S}}$).
$\Pi_{\mathcal{W}}$	One of the four special tangent planes to $\mathcal{W}$ (reciprocal to $\boldsymbol{c}_{\mathcal{S}}$).
$\mathcal{C}_{\mathcal{W}}$	One of the four circles in which $\Pi_{\mathcal{W}}$ touches $\mathcal{W}$.
$\mathcal{D}_{\mathcal{W}}$	The disk spanning $\mathcal{C}_{\mathcal{W}}$.
$\Sigma_{\pm}$, $\chi_{\pm}$	The two cones of internal conical refraction (vertex $\mathbf{0}$, base $\mathcal{C}_{\mathcal{W}}$), equation $\chi_{\pm}(\boldsymbol{x}) = 0$.
$\mathcal{L}$	Loop or loops forming the intersection of plane $\boldsymbol{\xi}\cdot\boldsymbol{x} = t$ with slowness surface $\mathcal{S}$.
$\boldsymbol{\nabla}$, $\dot{}$	Derivatives with respect to $\boldsymbol{x}$ and t.

Notes: 1) When used in matrix calculations vectors are columns unless explicitly transposed. (Thus $\boldsymbol{x}^T\boldsymbol{x}$ is a scalar and $\boldsymbol{x}\boldsymbol{x}^T$ is 3×3.) 2) There are four conical points $\boldsymbol{c}_{\mathcal{S}}$. $\boldsymbol{c}_{\mathcal{S}}$ in the singular refers to the $\boldsymbol{c}_{\mathcal{S}}$ in $\xi_1 > 0$, $\xi_3 > 0$. And similarly for some other quantities.

2 Crystal optics equations

2.1 Maxwell's equations and the slowness surface

We follow Born and Wolf (1991, Chapter XIV). Let $\boldsymbol{x} = (x_1, x_2, x_3) = (x, y, z)$ be Cartesian coordinates and t the time. Maxwell's equations and the constitutive equations of crystal optics are

$$\begin{aligned} -\frac{1}{c}\dot{\boldsymbol{B}} = \boldsymbol{\nabla} \times \boldsymbol{E}, \quad \frac{1}{c}\dot{\boldsymbol{D}} = \boldsymbol{\nabla} \times \boldsymbol{H}, \\ \boldsymbol{B} = \mu \boldsymbol{H}, \qquad \boldsymbol{D} = \boldsymbol{\epsilon}\boldsymbol{E}. \end{aligned} \tag{2.1}$$

Please refer to the Table of Notations for symbol definitions.

Since $\boldsymbol{E}$, $\boldsymbol{H}$, $\boldsymbol{D}$, and $\boldsymbol{B}$ may be expressed as superpositions of plane waves we shall seek them in a standard form for plane waves:

$$\begin{aligned} \boldsymbol{E} = \boldsymbol{e}\, f(t - \boldsymbol{\xi}\cdot\boldsymbol{x}), \quad \boldsymbol{H} = \boldsymbol{h}\, f(t - \boldsymbol{\xi}\cdot\boldsymbol{x}), \\ \boldsymbol{D} = \boldsymbol{d}\, f(t - \boldsymbol{\xi}\cdot\boldsymbol{x}), \quad \boldsymbol{B} = \boldsymbol{b}\, f(t - \boldsymbol{\xi}\cdot\boldsymbol{x}). \end{aligned} \tag{2.2}$$

Substitution of (2.2) into (2.1) leads to

$$\frac{1}{c}\boldsymbol{b} = \frac{\mu}{c}\boldsymbol{h} = \boldsymbol{\xi} \times \boldsymbol{e}, \quad -\frac{1}{c}\boldsymbol{d} = -\frac{\boldsymbol{\epsilon}}{c}\boldsymbol{e} = \boldsymbol{\xi} \times \boldsymbol{h}. \tag{2.3}$$

It easily follows that

$$\boldsymbol{\xi}\times(\boldsymbol{\xi}\times\boldsymbol{e}) = \frac{\mu}{c}\boldsymbol{\xi}\times\boldsymbol{h} = -\boldsymbol{\sigma e}, \tag{2.4}$$

i.e.

$$\boldsymbol{\sigma e} = |\boldsymbol{\xi}|^2\boldsymbol{e} - (\boldsymbol{\xi}\cdot\boldsymbol{e})\boldsymbol{\xi}. \tag{2.5}$$

Then from (2.3)

$$\boldsymbol{h}\cdot\boldsymbol{\xi} = \boldsymbol{b}\cdot\boldsymbol{\xi} = \boldsymbol{d}\cdot\boldsymbol{\xi} = \boldsymbol{e}\cdot\boldsymbol{h} = \boldsymbol{d}\cdot\boldsymbol{h} = 0. \tag{2.6}$$

Also

$$\begin{aligned}\boldsymbol{\xi}\cdot(\boldsymbol{e}\times\boldsymbol{h}) &= -\boldsymbol{e}\cdot(\boldsymbol{\xi}\times\boldsymbol{h}) = \boldsymbol{h}\cdot(\boldsymbol{\xi}\times\boldsymbol{e})\\ &= \frac{1}{c}\boldsymbol{e}\cdot\boldsymbol{d} = \frac{1}{c}\boldsymbol{h}\cdot\boldsymbol{b}.\end{aligned} \tag{2.7}$$

We shall often assume that

$$\epsilon_{ij} = \epsilon_i\delta_{ij}, \quad \sigma_{ij} = \sigma_i\delta_{ij}. \tag{2.8}$$

No summation is implied. Then

$$d_k = \epsilon_k e_k, \quad b_k = \mu h_k. \tag{2.9}$$

From (2.7) we have

$$\frac{1}{c}\sum_k \epsilon_k e_k^2 = \frac{1}{c}\mu|\boldsymbol{h}|^2 = \boldsymbol{\xi}\cdot(\boldsymbol{e}\times\boldsymbol{h}). \tag{2.10}$$

From (2.7),(2.8),(2.9) we obtain

$$\frac{\mu\epsilon_k}{c^2}e_k = |\boldsymbol{\xi}|^2 e_k - (\boldsymbol{\xi}\cdot\boldsymbol{e})\xi_k. \tag{2.11}$$

Writing

$$\sigma_k = \frac{\mu\epsilon_k}{c^2} \tag{2.12}$$

and rearranging (2.11) we get

$$e_k = (\boldsymbol{\xi}\cdot\boldsymbol{e})\frac{\xi_k}{|\boldsymbol{\xi}|^2 - \sigma_k}. \tag{2.13}$$

Equation (2.9) for d_k and (2.13) lead to

$$d_k = (\boldsymbol{\xi}\cdot\boldsymbol{e})\frac{\epsilon_k\xi_k}{|\boldsymbol{\xi}|^2 - \sigma_k}. \tag{2.14}$$

Contracting (2.13) with ξ_k and canceling $\boldsymbol{\xi}\cdot\boldsymbol{e}$ we obtain

$$\sum_k \frac{\xi_k^2}{|\boldsymbol{\xi}|^2 - \sigma_k} = 1. \tag{2.15}$$

Contracting (2.14) by ξ_k and using $\boldsymbol{\xi}\cdot\boldsymbol{d} = 0$ we get

$$\sum_k \frac{\sigma_k \xi_k^2}{|\boldsymbol{\xi}|^2 - \sigma_k} = 0. \tag{2.16}$$

Equations (2.15) and (2.16) may be taken as equivalent equations of the **slowness surface** $\mathcal{S}_{\boldsymbol{\sigma}}$ on which $\boldsymbol{\xi}$ is constrained to lie. Another equation for $\mathcal{S}$ is

$$\det(\boldsymbol{\sigma} - |\boldsymbol{\xi}|^2 \mathbf{1} + \boldsymbol{\xi}\boldsymbol{\xi}^T) = 0 \tag{2.17}$$

obtained from (2.5) regarded as a linear system in $\boldsymbol{e}$. In (2.17) $\mathbf{1}$ is the identity 3×3 tensor and $\boldsymbol{\xi}^T$ is the transpose of the column vector $\boldsymbol{\xi}$. Equation (2.17) can be written more explicitly as

$$|\boldsymbol{\xi}|^2 \, \boldsymbol{\xi}^T \boldsymbol{\sigma} \boldsymbol{\xi} - [\mathrm{tr}(\mathrm{adj}\boldsymbol{\sigma})|\boldsymbol{\xi}|^2 - \boldsymbol{\xi}^T \mathrm{adj}\boldsymbol{\sigma} \, \boldsymbol{\xi}] + \det \boldsymbol{\sigma} = 0, \tag{2.18}$$

where adj stands for the transposed matrix of cofactors, and tr for the trace; to obtain this equation, we use the principal axes of $\boldsymbol{\sigma}$ as coordinates, multiply out Equation (2.17) explicitly and identify certain combinations of quantities that are invariant and can be expressed as in (2.18). See Figure 1.

In the following we consider a uniform, homogeneous crystal, so that the principal values of the permittivity are positive and the corresponding hyperbolic system has fixed multiplicity.

2.2 The wave surface.

Let us now consider the wave surface reciprocal to the slowness surface. Remarkably for the system of crystal optics the algebraic form of the two surfaces is the same.

To see this we first consider the equation of energy conservation

$$\partial_t [\tfrac{1}{8\pi}(\boldsymbol{E} \cdot \boldsymbol{D} + \boldsymbol{H} \cdot \boldsymbol{B})] = -\tfrac{c}{4\pi} \boldsymbol{\nabla} \cdot (\boldsymbol{E} \times \boldsymbol{H}). \tag{2.19}$$

This is easily verified from equations (2.1). The quantity $\frac{1}{8\pi}(\boldsymbol{E} \cdot \boldsymbol{D} + \boldsymbol{H} \cdot \boldsymbol{B})$ is the energy density and $\frac{c}{4\pi} \boldsymbol{E} \times \boldsymbol{H}$ is the Poynting vector giving the power flux density. For plane waves $\boldsymbol{E} \cdot \boldsymbol{D} = \boldsymbol{H} \cdot \boldsymbol{B}$, and the Poynting vector is the group, or ray, velocity multiplied by the energy density. It follows by using (2.3) and (2.7) in (2.19) that

$$\tfrac{1}{8\pi}(\boldsymbol{e} \cdot \boldsymbol{d} + \boldsymbol{h} \cdot \boldsymbol{b}) = \tfrac{1}{4\pi} \boldsymbol{e} \cdot \boldsymbol{d} \;\; = \;\; \tfrac{1}{4\pi} \boldsymbol{h} \cdot \boldsymbol{b} = \tfrac{1}{4\pi} \mu |\boldsymbol{h}|^2 = \tfrac{c}{4\pi} \boldsymbol{\xi} \cdot (\boldsymbol{e} \times \boldsymbol{h}), \tag{2.20}$$

from which we may deduce that the ray velocity $\boldsymbol{v}$ is

$$\boldsymbol{v} = \frac{c}{4\pi} \frac{1}{\mu |\boldsymbol{h}|^2} \boldsymbol{e} \times \boldsymbol{h}. \tag{2.21}$$

For future reference let us notice here that from (2.6) and (2.21) the vectors $\boldsymbol{\xi}$, $\boldsymbol{v}$, $\boldsymbol{d}$, and $\boldsymbol{e}$ all lie in the same plane orthogonal to the parallel vectors $\boldsymbol{b}$, $\boldsymbol{h}$.

From (2.20), (2.21) we have

$$\boldsymbol{\xi} \cdot \boldsymbol{v} = 1. \tag{2.22}$$

We may now verify that

$$\boldsymbol{v}\times(\boldsymbol{v}\times\boldsymbol{d}) \;=\; -\boldsymbol{\sigma}^{-1}\boldsymbol{d}, \tag{2.23}$$

i.e.

$$\boldsymbol{\sigma}^{-1}\boldsymbol{d} = |\boldsymbol{v}|^2\boldsymbol{d} - (\boldsymbol{v}\cdot\boldsymbol{d})\boldsymbol{v}. \tag{2.24}$$

Taking advantage of the fact that $\boldsymbol{\sigma}$ is diagonal in the current coordinate system we may write (2.24) as

$$\frac{1}{\sigma_k}\,d_k = |\boldsymbol{v}|^2 d_k - (\boldsymbol{v}\cdot\boldsymbol{d})v_k, \tag{2.25}$$

leading to

$$\sum_k \frac{v_k^2}{|\boldsymbol{v}|^2 - \dfrac{1}{\sigma_k}} = 1, \qquad \sum_k \frac{\dfrac{1}{\sigma_k}v_k^2}{|\boldsymbol{v}|^2 - \dfrac{1}{\sigma_k}} = 0, \tag{2.26}$$

and

$$\det(\boldsymbol{\sigma}^{-1} - |\boldsymbol{v}|^2\mathbf{1} + \boldsymbol{v}\boldsymbol{v}^T) = 0; \tag{2.27}$$

compare (2.15), (2.16), (2.17). Also

$$|\boldsymbol{v}|^2\,\boldsymbol{v}^T\mathrm{adj}\boldsymbol{\sigma}\,\boldsymbol{v} - [\mathrm{tr}(\boldsymbol{\sigma})|\boldsymbol{v}|^2 - \boldsymbol{v}^T\boldsymbol{\sigma}\,\boldsymbol{v}] + 1 = 0, \tag{2.28}$$

in analogy with the development (2.11) to (2.17). Equations (2.26) and (2.27),(2.28) may be taken as equivalent equations of the **wave surface** $\mathcal{W}_{\boldsymbol{\sigma}}$ upon which $\boldsymbol{v}$ is constrained to lie. See Figures 2 and 3. Two cones $\Sigma_\pm$ having the origin as vertex pass through the circles. Their equations are

$$\chi_\pm(\boldsymbol{\xi}) \equiv (\xi_{c3}x_1 \pm \xi_{c1}x_3)\Big(\frac{\xi_{c3}x_1}{\sigma_1} \pm \frac{\xi_{c1}x_3}{\sigma_3}\Big) + x_2^2 = 0; \tag{2.29}$$

see Appendix A for the derivation of these equations.

3 The Cauchy problem

In this section we set up and solve the Cauchy problem for the second-order system of PDE's obtained by eliminating $\boldsymbol{B}$, $\boldsymbol{D}$, $\boldsymbol{H}$ from (2.1). Later we shall evaluate the solution numerically and present some results graphically. Our development is strongly motivated by John (1955), the discussion of the Herglotz-Petrovskii formula in Gelfand and Shilov (1964), and Petrovskii (1945).

3.1 The second-order equation for $\boldsymbol{E}$

The elimination of $\boldsymbol{B}$, $\boldsymbol{D}$, $\boldsymbol{H}$ from (2.1) yields the single second-order equation

$$\boldsymbol{\sigma}\ddot{\boldsymbol{E}} = -\boldsymbol{\nabla}\times\boldsymbol{\nabla}\times\boldsymbol{E} = (\boldsymbol{\nabla}^2\mathbf{1} - \boldsymbol{\nabla}\boldsymbol{\nabla}^T)\boldsymbol{E}. \tag{3.1}$$

Then, on writing ∂_t for $\partial/\partial t$ (3.1) becomes

$$[\sigma\partial_t^2 - P(\boldsymbol{\nabla})]\boldsymbol{E} = 0, \tag{3.2}$$

where

$$P(\boldsymbol{\xi}) = |\boldsymbol{\xi}|^2\mathbf{1} - \boldsymbol{\xi}\boldsymbol{\xi}^T, \tag{3.3}$$

so that $P(\hat{\boldsymbol{\xi}})$ is the projection onto the plane normal to $\hat{\boldsymbol{\xi}}$. We shall generate the fundamental solution of (3.2) by solving the Cauchy problem for (3.2) in $t > 0$ with initial conditions

$$\boldsymbol{E}(x, 0) = 0, \quad \partial_t\boldsymbol{E}(x, 0) = \boldsymbol{\sigma}^{-1}\delta(\boldsymbol{x}), \tag{3.4}$$

where

$$\delta(\boldsymbol{x}) = \delta(x_1)\delta(x_2)\delta(x_3). \tag{3.5}$$

By Duhamel's principle this Cauchy problem is equivalent to the inhomogeneous equation

$$[\boldsymbol{\sigma}\partial_t^2 - P(\boldsymbol{\nabla})]\boldsymbol{E} = \mathbf{1}\delta(t)\delta(\boldsymbol{x}), \tag{3.6}$$

with $\boldsymbol{E} = 0$ for $t < 0$. We shall solve this using the following considerations, which are motivated by John (1955), Chapter 2; in addition, we generalize that work to a matrix formulation and consider the degenerate mode with zero wave speed.

3.2 The residue calculation

Let us write

$$L(v, \boldsymbol{\xi}) = v^2\boldsymbol{\sigma} - P(\boldsymbol{\xi}), \tag{3.7}$$

regarding v as a scalar complex variable. Then for large enough $|v|$

$$\begin{aligned} L^{-1}(v, \boldsymbol{\xi}) &= v^{-2}\boldsymbol{\sigma}^{-1}[\mathbf{1} - v^{-2}P(\boldsymbol{\xi})\boldsymbol{\sigma}^{-1}]^{-1} \\ &= v^{-2}\boldsymbol{\sigma}^{-1}\sum_{n=0}^{\infty} v^{-2n}(P(\boldsymbol{\xi})\boldsymbol{\sigma}^{-1})^n. \end{aligned} \tag{3.8}$$

This is a series in inverse even powers of v, starting with v^{-2}. On multiplying this by v^q and integrating around a large circle centered at the origin in the complex v plane we obtain

$$I = \frac{1}{2\pi\mathrm{i}}\oint L^{-1}(v, \boldsymbol{\xi})v^q \,\mathrm{d}v = \begin{cases} 0, & q = 0, \\ \boldsymbol{\sigma}^{-1}, & q = 1. \end{cases} \tag{3.9}$$

Other values of q will not concern us. Let us now evaluate I by residues at the finite poles. When $\xi \neq 0$ there are four simple non-zero poles $\pm V_1$, $\pm V_2$ of L^{-1} and a double pole at $v = 0$. Thus, if we write V_{-1} for $-V_1$ and V_{-2} for $-V_2$, and ∂_v for $\partial/\partial v$ we find on evaluating the residues at the V_N that

$$I = \sum_N \frac{v^q \mathrm{adj}\, L}{\partial_v \det L}\bigg|_{v=V_N} + \quad \{\text{residue at } v = 0\}. \tag{3.10}$$

We may rewrite $\partial_v \det L|_{v=V_N}$ as

$$\partial_v \det L|_{v=V_N} = \partial_v \det(v^2\boldsymbol{\sigma} - P)|_{v=V_N} = 2V_N \mathrm{tr}(\boldsymbol{\sigma}\, \mathrm{adj} L). \tag{3.11}$$

To find the residue at $v = 0$ we expand $(v^2\boldsymbol{\sigma} - P)^{-1}$ in positive powers of v. Thus using

$$\mathrm{adj} P(\boldsymbol{\xi}) = |\boldsymbol{\xi}|^2 \boldsymbol{\xi}\boldsymbol{\xi}^T \tag{3.12}$$

we find that

$$\begin{aligned} \det L &= \mathrm{adj}(v^2\boldsymbol{\sigma} - P) \\ &= \mathrm{adj} P + O(|v|^2) \\ &= |\boldsymbol{\xi}|^2 \boldsymbol{\xi}\boldsymbol{\xi}^T + O(|v|^2). \end{aligned} \tag{3.13}$$

Recalling that $\det P = 0$ we see that

$$\begin{aligned} \det(v^2\boldsymbol{\sigma} - P) &= v^2 \mathrm{tr}(\boldsymbol{\sigma} \mathrm{adj} P) + O(|v|^4) \\ &= v^2 |\boldsymbol{\xi}|^2\, \boldsymbol{\xi}^T \boldsymbol{\sigma} \boldsymbol{\xi} + O(|v|^4). \end{aligned} \tag{3.14}$$

So

$$\{\det[L(v, \boldsymbol{\xi}))]\}^{-1} = \frac{v^{-2}}{|\boldsymbol{\xi}|^2\, \boldsymbol{\xi}^T \boldsymbol{\sigma} \boldsymbol{\xi}} + O(1). \tag{3.15}$$

Thus the residue of $v^q L^{-1}$ at 0 is

$$\{\text{residue of } v^q L^{-1} \text{at } v = 0\} = \begin{cases} 0, & q = 0, \\ \dfrac{\boldsymbol{\xi}\boldsymbol{\xi}^T}{\boldsymbol{\xi}^T \boldsymbol{\sigma} \boldsymbol{\xi}}, & q = 1. \end{cases} \tag{3.16}$$

Thus, from (3.9), (3.10), (3.11), and (3.16) we find that

$$\sum_N \frac{\mathrm{adj} L_N}{2V_N \mathrm{tr}(\boldsymbol{\sigma} \mathrm{adj} L_N)} = 0, \tag{3.17}$$

and

$$\sum_N \frac{\mathrm{adj} L_N}{2\,\mathrm{tr}(\boldsymbol{\sigma} \mathrm{adj} L_N)} + \frac{\boldsymbol{\xi}\boldsymbol{\xi}^T}{\boldsymbol{\xi}^T \boldsymbol{\sigma} \boldsymbol{\xi}} = \boldsymbol{\sigma}^{-1}. \tag{3.18}$$

Here we have written L_N for L evaluated at $v = V_N$, $N = \pm 1, \pm 2$.

3.3 The fundamental solution

Let us first seek a matrix plane-wave solution G_ξ of (3.2) in the form

$$G_\xi(\boldsymbol{x}, t) = \sum_N \frac{\mathrm{adj} L_N}{2V_N \mathrm{tr}(\boldsymbol{\sigma} \mathrm{adj} L_N)} f(V_N t - \boldsymbol{\xi}\cdot\boldsymbol{x}) + \frac{\boldsymbol{\xi}\boldsymbol{\xi}^T}{\boldsymbol{\xi}^T \boldsymbol{\sigma} \boldsymbol{\xi}} t f'(-\boldsymbol{\xi}\cdot\boldsymbol{x}). \tag{3.19}$$

This form is motivated by the plane wave decomposition of the δ-function, (3.23), and the above results of the residue calculation, (3.18).

We first verify that $L(\partial_t, \boldsymbol{\nabla})G_\xi(\boldsymbol{x}, t) = 0$. Thus

$$\begin{aligned} L(\partial_t, \boldsymbol{\nabla})G_\xi(\boldsymbol{x}, t) &= \sum_N \frac{L_N \mathrm{adj} L_N}{2V_N \mathrm{tr}(\boldsymbol{\sigma}\mathrm{adj}L_N)} f''(V_N t - \boldsymbol{\xi}\cdot\boldsymbol{x}) \\ &= \sum_N \frac{\det L_N \, \mathbf{1}}{2V_N \mathrm{tr}(\boldsymbol{\sigma}\mathrm{adj}L_N)} f''(V_N t - \boldsymbol{\xi}\cdot\boldsymbol{x}) \\ &= 0, \end{aligned} \tag{3.20}$$

since each $\det L_N = 0$. By (3.17) the initial value of G_ξ is

$$G_\xi(\boldsymbol{x}, 0) = \sum_N \frac{\mathrm{adj}L_N}{2V_N \mathrm{tr}(\boldsymbol{\sigma}\mathrm{adj}L_N)} f(-\boldsymbol{\xi}\cdot\boldsymbol{x}) = 0, \tag{3.21}$$

and by (3.18) the initial value of $\partial_t G_\xi$ is

$$\partial_t G_\xi(\boldsymbol{x}, 0) = \sum_N \frac{\mathrm{adj}L_N}{2\,\mathrm{tr}(\boldsymbol{\sigma}\mathrm{adj}L_N)} f'(-\boldsymbol{\xi}\cdot\boldsymbol{x}) + \frac{\boldsymbol{\xi}\boldsymbol{\xi}^T}{\boldsymbol{\xi}^T\boldsymbol{\sigma}\boldsymbol{\xi}} f'(-\boldsymbol{\xi}\cdot\boldsymbol{x}) = \boldsymbol{\sigma}^{-1} f'(-\boldsymbol{\xi}\cdot\boldsymbol{x}). \tag{3.22}$$

We are ultimately interested in the matrix point source problem (3.2), (3.4), (3.5) or equivalently (3.6). The link is the plane-wave expansion of the δ-function,

$$\delta(\boldsymbol{x}) = -\frac{1}{8\pi^2}\int_\Omega \delta''(\hat{\boldsymbol{\xi}}\cdot\boldsymbol{x})\,\mathrm{d}\Omega, \tag{3.23}$$

where Ω is the unit sphere $|\boldsymbol{\xi}| = 1$, $\mathrm{d}\Omega$ is the surface element on Ω, and δ'' is the second derivative of the one-dimensional δ-function. (See John, 1955, Chapter II; Courant and Hilbert, 1962, Chapter VI, Section 11; and Gelfand and Shilov, 1964, Chapter I, Section 3.11.) From (3.21) and (3.22), and setting $f = \delta'$, we see that

$$\begin{aligned} G(\boldsymbol{x}, t) &= -\frac{1}{8\pi^2}\int_\Omega G_\xi(\boldsymbol{x}, t)\,\mathrm{d}S \\ &= -\frac{1}{8\pi^2}\sum_N \int_\Omega \frac{\mathrm{adj}L_N}{2V_N \mathrm{tr}(\boldsymbol{\sigma}\mathrm{adj}L_N)} \delta'(V_N t - \hat{\boldsymbol{\xi}}\cdot\boldsymbol{x})\,\mathrm{d}\Omega - \frac{t}{8\pi^2}\int_\Omega \frac{\hat{\boldsymbol{\xi}}\hat{\boldsymbol{\xi}}^T}{\hat{\boldsymbol{\xi}}^T\boldsymbol{\sigma}\hat{\boldsymbol{\xi}}}\,\delta''(-\hat{\boldsymbol{\xi}}\cdot\boldsymbol{x})\,\mathrm{d}\Omega \end{aligned} \tag{3.24}$$

satisfies (3.4) exactly.

3.4 Transformation to an integral over the slowness surface

Here we follow John (1955, Chapter II) and Gelfand and Shilov (1964, Chapter I, Section 6.3). If the wave-speeds $\pm V_N$ are ordered from the most negative to the most positive we find that $V_N(-\boldsymbol{\xi}) = V_{-N}(\boldsymbol{\xi})$. This and the fact that the V_N are homogeneous functions of degree 1 imply that the integral in (3.24) for N is the same as the integral for $-N$. Thus we may combine the terms for $\pm N$ and write

$$G(\boldsymbol{x},t) = -\frac{1}{4\pi^2}\sum_{N=1,2}\int_\Omega \frac{\mathrm{adj}L_N}{2V_N\mathrm{tr}(\boldsymbol{\sigma}\mathrm{adj}L_N)}\delta'(V_N t-\hat{\boldsymbol{\xi}}\cdot\boldsymbol{x})\,\mathrm{d}\Omega - \frac{1}{8\pi^2}\int_\Omega \frac{\hat{\boldsymbol{\xi}}\hat{\boldsymbol{\xi}}^T}{\hat{\boldsymbol{\xi}}^T\boldsymbol{\sigma}\hat{\boldsymbol{\xi}}} t\,\delta''(-\hat{\boldsymbol{\xi}}\cdot\boldsymbol{x})\,\mathrm{d}\Omega. \tag{3.25}$$

In the Nth term of (3.24) let us transform the integral over Ω to one over S_N, $N = 1, 2$, where S_N is the sheet of the slowness surface corresponding to slowness $\frac{1}{V_N(\hat{\boldsymbol{\xi}})}$. We note that

$$|\boldsymbol{\xi}|^2\,\mathrm{d}\Omega = \cos\theta\,\mathrm{d}S_N = \frac{\boldsymbol{\xi}\cdot\boldsymbol{\nabla}_\xi V_N}{|\boldsymbol{\xi}|\,|\boldsymbol{\nabla}_\xi V_N|}\,\mathrm{d}S_N = \frac{1}{|\boldsymbol{\xi}|\,|\boldsymbol{\nabla}_\xi V_N|}\,\mathrm{d}S_N, \tag{3.26}$$

where $\boldsymbol{\xi} = |\boldsymbol{\xi}|\hat{\boldsymbol{\xi}}$, θ is the angle between $\boldsymbol{\xi}$ and $\hat{\boldsymbol{v}}$ the normal to S_N, and $\mathrm{d}S_N$ is the surface element on S_N and we have used the homogeneity of V_N as a function of $\boldsymbol{\xi}$. We next use the facts that $V_N(\boldsymbol{\xi}) = 1$ on S_N, δ' is homogeneous of degree -2, and that $V_N(\boldsymbol{\xi})$ is homogeneous of degree 1, to get

$$\frac{\delta'(V_N(\hat{\boldsymbol{\xi}})t - \hat{\boldsymbol{\xi}}\cdot\boldsymbol{x})}{V_N(\hat{\boldsymbol{\xi}})} \;=\; |\boldsymbol{\xi}|^3\frac{\delta'(V_N(\boldsymbol{\xi})t - \boldsymbol{\xi}\cdot\boldsymbol{x})}{V_N(\boldsymbol{\xi})} = |\boldsymbol{\xi}|^3\delta'(t - \boldsymbol{\xi}\cdot\boldsymbol{x}). \tag{3.27}$$

Finally we write

$$G(\boldsymbol{x},t) \;=\; -\frac{1}{8\pi^2}\partial_t\int_{\mathcal{S}}\frac{\mathrm{adj}L(1,\boldsymbol{\xi})\delta(t-\boldsymbol{\xi}\cdot\boldsymbol{x})}{|\boldsymbol{\nabla}_\xi V_N|\,\mathrm{tr}[\boldsymbol{\sigma}\,\mathrm{adj}L(1,\boldsymbol{\xi})]}\,\mathrm{d}S - \frac{t}{8\pi^2}\int_\Omega \frac{\hat{\boldsymbol{\xi}}\hat{\boldsymbol{\xi}}^T\delta''(\hat{\boldsymbol{\xi}}\cdot\boldsymbol{x})}{\hat{\boldsymbol{\xi}}^T\boldsymbol{\sigma}\hat{\boldsymbol{\xi}}}\,\mathrm{d}\Omega, \tag{3.28}$$

where we have combined the two terms $N = 1, 2$ by integrating over the whole of $\mathcal{S}$ which comprises both sheets. Because of the properties of δ the integrals may be written as integrals along curves of intersection of the algebraic surface $\mathcal{S}$ with the plane $\boldsymbol{\xi}\cdot\boldsymbol{x} = t$. We shall elucidate this and make more explicit the various expressions appearing in the integrand.

One may also examine the above fundamental solution from a microlocal point of view. For example, one may use Fourier Integral Operator theory to construct the parametrix for the Cauchy problem to study singularities, which eventually leads to the Herglotz-Petrovskii formula for the fundamental solution of the hyperbolic system under consideration (Hörmander, 1980; Chapter 12); however, here we will not pursue this line further.

4 The loop integrals

Consider the integral expression of (3.28) repeated here for convenience

$$G(\boldsymbol{x},t) \;=\; -\frac{1}{8\pi^2}\partial_t\int_{\mathcal{S}}\frac{\mathrm{adj}L(1,\boldsymbol{\xi})\delta(t-\boldsymbol{\xi}\cdot\boldsymbol{x})}{|\boldsymbol{\nabla}_\xi v|\,\mathrm{tr}[\boldsymbol{\sigma}\,\mathrm{adj}L(1,\boldsymbol{\xi})]}\,\mathrm{d}S - \frac{t}{8\pi^2}\int_\Omega \frac{\hat{\boldsymbol{\xi}}\hat{\boldsymbol{\xi}}^T\delta''(\hat{\boldsymbol{\xi}}\cdot\boldsymbol{x})}{\hat{\boldsymbol{\xi}}^T\boldsymbol{\sigma}\hat{\boldsymbol{\xi}}}\,\mathrm{d}\Omega. \tag{4.1}$$

The first integral reduces to an integral around a curve, the intersection of $\mathcal{S}$ and the plane $\boldsymbol{\xi}\cdot\boldsymbol{x} = t$. Let $\boldsymbol{n}$ be the outward unit normal to $\mathcal{S}$ and ζ' defined by

$$\zeta' = \hat{\boldsymbol{x}}\cdot\boldsymbol{\xi}. \tag{4.2}$$

Then

$$\sin\theta \, \mathrm{d}\mathcal{S} = \, \mathrm{d}s \, \mathrm{d}\zeta', \tag{4.3}$$

where s is arc-length along the curve and

$$\cos\theta = \hat{\boldsymbol{x}}\cdot\boldsymbol{n} = \frac{\hat{\boldsymbol{x}}\cdot\boldsymbol{\nabla}_\xi v}{|\boldsymbol{\nabla}_\xi v|}. \tag{4.4}$$

Hence

$$\frac{\delta(t-\boldsymbol{\xi}\cdot\boldsymbol{x})\,\mathrm{d}\mathcal{S}}{|\boldsymbol{\nabla}_\xi v|} = \frac{\delta(t-|\boldsymbol{x}|\,\zeta')\,\mathrm{d}s\,\mathrm{d}\zeta'}{\sqrt{|\boldsymbol{\nabla}_\xi v|^2-(\hat{\boldsymbol{x}}\cdot\boldsymbol{\nabla}_\xi v)^2}}. \tag{4.5}$$

Thus

$$\int_{\mathcal{S}} \frac{\mathrm{adj}L(1,\boldsymbol{\xi})\delta(t-\boldsymbol{\xi}\cdot\boldsymbol{x})}{|\boldsymbol{\nabla}_\xi v|\,\mathrm{tr}[\boldsymbol{\sigma}\,\mathrm{adj}L(1,\boldsymbol{\xi})]}\,\mathrm{d}\mathcal{S} = \frac{1}{|\boldsymbol{x}|}\int_{\mathcal{L}} \frac{\mathrm{adj}L(1,\boldsymbol{\xi})\,\mathrm{d}s}{\mathrm{tr}[\boldsymbol{\sigma}\,\mathrm{adj}L(1,\boldsymbol{\xi})]\sqrt{|\boldsymbol{\nabla}_\xi v|^2-(\hat{\boldsymbol{x}}\cdot\boldsymbol{\nabla}_\xi v)^2}}. \tag{4.6}$$

Here $\mathcal{L}$ is the complete real intersection of $\mathcal{S}$ with the plane $\boldsymbol{\xi}\cdot\boldsymbol{x} = t$ and $\mathrm{d}s$ is arc-length along $\mathcal{L}$.

4.1 Implicit computation of complete intersection $\mathcal{L}$

To evaluate the integral (4.6), we have to compute the complete real intersection $\mathcal{L}$ of $\mathcal{S}$ with the plane $\boldsymbol{\xi}\cdot\boldsymbol{x} = t$. We use an Eulerian approach.

Since

$$\mathcal{S} = \{\xi \in R^3 : \det(\boldsymbol{\sigma} - P(\boldsymbol{\xi})) = 0\}, \tag{4.7}$$

we define the function

$$\Phi(\xi) \equiv \det(\boldsymbol{\sigma} - P(\boldsymbol{\xi})), \tag{4.8}$$

and find its zero level set $\mathcal{S}$:

$$\mathcal{S} = \{\boldsymbol{\xi} \in R^3 : \Phi(\boldsymbol{\xi}) = 0\}. \tag{4.9}$$

Moreover, the hyperplane $\boldsymbol{\xi}\cdot\boldsymbol{x} = t$ may also be represented implicitly by the zero level set of function

$$\Psi(\boldsymbol{\xi}) \equiv \boldsymbol{\xi}\cdot\boldsymbol{x} - t. \tag{4.10}$$

To reduce the computational complexity, we use the fact that $\mathcal{L}$ always lies on the plane $\boldsymbol{\xi}\cdot\boldsymbol{x} = t$ with a fixed normal $\hat{\boldsymbol{x}}$. Thus we may rotate the coordinate system first and find $\mathcal{L}$ by contouring zero level sets of a 2-dimensional function. This technique is commonly used in the level set method for dynamic implicit surfaces; see Osher and Fedkiw (2002).

In the numerical implementation, we have used linear interpolation for contouring zero level sets and trapezoid quadrature for numerical integration so that the computed fundamental solution has at least second-order accuracy in terms of mesh size used for contouring zero level sets; on the other hand, we may use the Newton-Raphson method to improve the accuracy for contouring zero level sets, which is not carried out here.

4.2 The method of evaluation

The method of numerical evaluation is as follows. We first rotate the coordinate system so that the new 3-direction is parallel to $\boldsymbol{x}$. Thus, defining the rotation matrix Q to have $\hat{\boldsymbol{x}}$ as its third column (We chose the second column to lie in the 12-plane.), and setting

$$\boldsymbol{\xi} = Q\,\boldsymbol{\xi}' \tag{4.11}$$

the coordinate ξ_3' is in the direction of $\boldsymbol{x}$ as required and ξ_1', ξ_2', ξ_3' form a right-handed orthogonal coordinate system. So, using

$$\boldsymbol{\sigma}' = Q^T\boldsymbol{\sigma}Q, \quad \boldsymbol{\xi}' = Q^T\boldsymbol{\xi} \tag{4.12}$$

we may write the determinant $\det\{\boldsymbol{\sigma} - P(\boldsymbol{\xi})\}$ as

$$\det\{\boldsymbol{\sigma} - P(\boldsymbol{\xi})\} = \det\{\boldsymbol{\sigma}' - P(\boldsymbol{\xi}')\} = \sigma_1\sigma_2\sigma_3 - \mathrm{tr}\{\mathrm{adj}(\boldsymbol{\sigma}'\}|\boldsymbol{\xi}'|^2 + \boldsymbol{\xi}'^T\mathrm{adj}(\boldsymbol{\sigma}')\boldsymbol{\xi}' + |\boldsymbol{\xi}'|^2\boldsymbol{\xi}'^T\boldsymbol{\sigma}'\boldsymbol{\xi}' \tag{4.13}$$

as a function of ξ_1' and ξ_2' for each fixed $\xi_3' = t/|\boldsymbol{x}|$. A Matlab code was written using the `contour` command to find $\mathcal{L}$ as a curve or curves of points in the $\xi_1'\xi_2'$-plane where this determinant vanishes. The integration was performed to second order accuracy in the mesh size on which $\det\{\boldsymbol{\sigma}' - P(\boldsymbol{\xi}')\}$ was evaluated.

5 The static term

In (3.28) the final term of the fundamental solution G represents a non-propagating disturbance, corresponding to zero velocity, which grows linearly in time and is singular at the origin. It is

$$J(\boldsymbol{x},t) = -\frac{t}{8\pi^2}\int_\Omega \frac{\hat{\boldsymbol{\xi}}\hat{\boldsymbol{\xi}}^T}{\hat{\boldsymbol{\xi}}^T\boldsymbol{\sigma}\hat{\boldsymbol{\xi}}}\delta''(\hat{\boldsymbol{\xi}}\cdot\boldsymbol{x})\,\mathrm{d}\Omega. \tag{5.1}$$

Let us now calculate $J(\boldsymbol{x},t)$.

Let $\hat{\boldsymbol{x}}$ be the unit vector in the direction of $\boldsymbol{x}$ and let $\hat{\boldsymbol{y}}$, $\hat{\boldsymbol{z}}$ be chosen so that $\hat{\boldsymbol{x}}$, $\hat{\boldsymbol{y}}$, $\hat{\boldsymbol{z}}$ form a right-handed orthonormal triple.

Then a general unit vector $\hat{\boldsymbol{\xi}}$ perpendicular to $\boldsymbol{x}$ may be written as $\cos\phi\hat{\boldsymbol{y}} + \sin\phi\hat{\boldsymbol{z}}$, and we may write J as

$$J(\boldsymbol{x},t) = -\frac{t}{8\pi^2|\boldsymbol{x}|^3}\int_{-1}^{1}\int_0^{2\pi} \frac{\hat{\boldsymbol{\xi}}\hat{\boldsymbol{\xi}}^T}{\hat{\boldsymbol{\xi}}^T\boldsymbol{\sigma}\hat{\boldsymbol{\xi}}}\,\delta''(\mu)\,\mathrm{d}\phi\,\mathrm{d}\mu, \tag{5.2}$$

where

$$\hat{\boldsymbol{\xi}} \;=\; \mu\hat{\boldsymbol{x}} + \sqrt{1-\mu^2}(\cos\phi\hat{\boldsymbol{y}} + \sin\phi\hat{\boldsymbol{z}}), \tag{5.3}$$

and $\boldsymbol{x}^\perp = \cos\phi\hat{\boldsymbol{y}} + \sin\phi\hat{\boldsymbol{z}}$. Then

$$J(\boldsymbol{x},t) = -\frac{t}{8\pi^2|\boldsymbol{x}|^3}\int_0^{2\pi}\frac{\partial^2}{\partial\mu^2}\left(\frac{\hat{\boldsymbol{\xi}}\hat{\boldsymbol{\xi}}^T}{\hat{\boldsymbol{\xi}}^T\boldsymbol{\sigma}\hat{\boldsymbol{\xi}}}\right)\Bigg|_{\mu=0}\mathrm{d}\phi. \tag{5.4}$$

After some elementary calculations one finds that

$$\frac{\partial^2}{\partial\mu^2}\left(\frac{\hat{\boldsymbol{\xi}}\hat{\boldsymbol{\xi}}^T}{\hat{\boldsymbol{\xi}}^T\boldsymbol{\sigma}\hat{\boldsymbol{\xi}}}\right)\Big|_{\mu=0} = 2\left[\frac{\hat{\boldsymbol{x}}\hat{\boldsymbol{x}}^T}{\boldsymbol{x}^{\perp T}\boldsymbol{\sigma}\boldsymbol{x}^{\perp}} - \frac{2(\boldsymbol{x}^{\perp T}\boldsymbol{\sigma}\hat{\boldsymbol{x}})(\hat{\boldsymbol{x}}\boldsymbol{x}^{\perp T}+\boldsymbol{x}^{\perp}\hat{\boldsymbol{x}}^T)}{(\boldsymbol{x}^{\perp T}\boldsymbol{\sigma}\boldsymbol{x}^{\perp})^2} + \frac{4(\hat{\boldsymbol{x}}^T\boldsymbol{\sigma}\boldsymbol{x}^{\perp})^2\boldsymbol{x}^{\perp}\boldsymbol{x}^{\perp T}}{(\boldsymbol{x}^{\perp T}\boldsymbol{\sigma}\boldsymbol{x}^{\perp})^3}\right]. \tag{5.5}$$

Thus we need integrals of the form

$$I^{(0)} = \int_0^{2\pi}\frac{\mathrm{d}\phi}{D}, I^{(2)}_{pq} = \int_0^{2\pi}\frac{x^{\perp}_p x^{\perp}_q\,\mathrm{d}\phi}{D^2}, I^{(4)}_{pqrs} = \int_0^{2\pi}\frac{x^{\perp}_p x^{\perp}_q x^{\perp}_r x^{\perp}_s\,\mathrm{d}\phi}{D^3}, \tag{5.6}$$

where $D = \boldsymbol{x}^{\perp T}\boldsymbol{\sigma}\boldsymbol{x}^{\perp}$ and the superscripts indicate the ranks of the tensors. We begin with $I^{(0)}$ from which the others may be derived by means of

$$I^{(2)}_{pq} = -\frac{\partial I^{(0)}}{\partial\sigma_{pq}}, \quad I^{(4)}_{pqrs} = \frac{1}{2}\frac{\partial^2 I^{(0)}}{\partial\sigma_{pq}\partial\sigma_{rs}}. \tag{5.7}$$

Let us write

$$F = \hat{\boldsymbol{x}}^T\mathrm{adj}\boldsymbol{\sigma}\hat{\boldsymbol{x}}. \tag{5.8}$$

Then it may be shown that

$$I^{(0)} \;=\; \frac{2\pi}{F^{\frac{1}{2}}}; \tag{5.9}$$

see Appendix B. Let us further define

$$Z_{jk} = \epsilon_{ijk}\hat{x}_i, \quad \mathbf{w} = \boldsymbol{\sigma}\hat{\boldsymbol{x}}, \quad W = Z^T\boldsymbol{\sigma}Z. \tag{5.10}$$

Then, it follows after some further calculation that the static term of (3.28) is given by

$$\begin{aligned}&-\frac{t}{8\pi^2}\int_\Omega \frac{\hat{\boldsymbol{\xi}}\hat{\boldsymbol{\xi}}^T}{\hat{\boldsymbol{\xi}}^T\boldsymbol{\sigma}\hat{\boldsymbol{\xi}}}\,\delta''(\hat{\boldsymbol{\xi}}\cdot\boldsymbol{x})\,\mathrm{d}\Omega = \\ &-\frac{t}{4\pi F^{\frac{1}{2}}|\boldsymbol{x}|^3}\left\{2\hat{\boldsymbol{x}}\hat{\boldsymbol{x}}^T - \frac{\hat{\boldsymbol{x}}^T\boldsymbol{\sigma}\hat{\boldsymbol{x}}}{F}W - \frac{2}{F}(\hat{\boldsymbol{x}}\mathbf{w}^TW + W\mathbf{w}\hat{\boldsymbol{x}}^T) - \frac{2}{F}Z^T\mathbf{w}\mathbf{w}^TZ + \frac{3}{F^2}(\mathbf{w}^TW\mathbf{w})W\right\},\end{aligned} \tag{5.11}$$

with Z, $\mathbf{w}$, and W given by (5.10), and F by (5.8); see Appendix B.

We now have the ingredients for evaluating the solution G given in (3.28).

The field near the edge of the disk of tangency on the wavefront is difficult to express uniformly in the asymptotic sense, and so is the field near the conical points on the wavefront; however, they can be computed independently. Therefore, we have chosen to evaluate the fundamental solution numerically. One may evaluate the fundamental solution in the space-frequency domain based on Fourier analysis; here we prefer to evaluate the fundamental solution in the space-time domain because this domain is much closer to the physics and yields much simpler expressions at caustics (Burridge, 1995)). The resulting numerical method is flexible for concentrating on the specific regions that we are interested in.

6 The field in the 13-plane

In this section we plot the solution $G_{ij}(\boldsymbol{x},t)$ as functions of t for various fixed $\boldsymbol{x}$ with $|\boldsymbol{x}|=1$ and $\boldsymbol{x}$ given by

$$\boldsymbol{x}(\theta)=\begin{pmatrix}\sin\theta\\0\\\cos\theta\end{pmatrix}, \tag{6.1}$$

and $\theta=0,\pi/36,\pi/18,\ldots,\pi/2$, i.e. θ increasing by steps of 5° from 0° to 90°. This will give a sampling of points on the 13-plane illustrating the various types of behavior in relation to the geometrical configuration described at the end of the previous section. For clarity in the graphical illustrations we set the parameters to be σ_1=2.25, σ_2=1.0, σ_3=0.25; these parameters do not correspond to any real crystal.

Let us first define θ_a, θ_b and θ_c by

$$\begin{aligned}\tan\theta_a &= \sqrt{\frac{\sigma_3(\sigma_1-\sigma_2)}{\sigma_1(\sigma_2-\sigma_3)}},\\ \tan\theta_b &= \sqrt{\frac{\sigma_1(\sigma_1-\sigma_2)}{\sigma_3(\sigma_2-\sigma_3)}},\\ \tan\theta_c &= \sqrt{\frac{\sigma_1-\sigma_2}{\sigma_2-\sigma_3}}.\end{aligned} \tag{6.2}$$

Here θ_a and θ_b are the points at which the circle $\mathcal{C}_{\mathcal{S}}$ crosses the 13-plane, for $\theta=\theta_c$ $\boldsymbol{x}$ is parallel to a bi-radial and so points in the direction of the conical point $\mathcal{C}_{\mathcal{W}}$. We find that $\theta_a<\theta_c<\theta_b$. See Figure 4.

To understand the sequence of arrivals for a given θ draw the ray through the origin in the direction of $\boldsymbol{x}(\theta)$ in Figure 4. Now trace along the ray from the outside of $\mathcal{W}$ inward. Each crossing of the curves drawn is associated with the arrival of a singularity. A normal to $\mathcal{W}$ at one of these crossings gives the direction of the associated stationary point $\boldsymbol{\xi}_{1,2}$ on $\mathcal{S}$. Reciprocally the normal to $\mathcal{S}$ at such a $\boldsymbol{\xi}_{1,2}$ gives the direction of the point $\boldsymbol{x}$ to which it corresponds. Thus at both stationary points $\boldsymbol{\xi}_{1,2}$ corresponding to the ray in the direction of $\hat{\boldsymbol{x}}$ the normals to $\mathcal{S}$ have the same direction making an angle θ with the 3-axis. The inner sheet of $\mathcal{W}$ corresponds to the outer sheet of $\mathcal{S}$, and vice-versa as indicated in the captions to Figures 2 & 3.

For $0<\theta<\theta_a$ and again for $\theta_b<\theta<\pi/2$, the singularities all correspond to points of tangency on $\mathcal{S}$ with positive Gaussian curvature. These singularities are of the form

$$\frac{A(\hat{\boldsymbol{x}})\hat{\boldsymbol{e}}_{1,2}\hat{\boldsymbol{e}}_{1,2}^T}{K^{\frac{1}{2}}(\boldsymbol{\xi}_{1,2})|\boldsymbol{x}|}\delta[t-t_{1,2}(\theta)], \tag{6.3}$$

except for those $\boldsymbol{x}$ having directions passing too close to $\theta=\theta_a$ or θ_b, where the contact circle $\mathcal{C}_{\mathcal{W}}$ on the wave front crosses the 13-plane. In (6.3) A is a smoothly varying function of direction, $\boldsymbol{\xi}_{1,2}=\boldsymbol{\xi}_{1,2}(\theta)$ is one of the two points at which the plane $\boldsymbol{\xi}\cdot\boldsymbol{x}(\theta)=t$ is tangent to $\mathcal{S}$, and $t_{1,2}(\theta)$ the two corresponding values of t, with indexing such that $t_1<t_2$, and

$\boldsymbol{e}_{1,2}(\theta)$ is the corresponding polarization for $\boldsymbol{E}$. Then $\boldsymbol{\xi}_1(\theta)$ lies on the inner sheet of $\mathcal{S}$ and $\boldsymbol{\xi}_2(\theta)$ lies on the outer. See Figures 4 & 5. $K(\boldsymbol{\xi}_{1,2}) > 0$ is the Gaussian curvature of $\mathcal{S}$ at $\boldsymbol{\xi}_{1,2}$. See Burridge (1967).

For $\theta = \theta_a$, $\boldsymbol{\xi}_1 = \boldsymbol{c}_{\mathcal{S}}$ and $\boldsymbol{\xi}_2$ is on the outer sheet still near the 3-axis.

For $\theta_a < \theta < \theta_c$ and for $\theta_c < \theta < \theta_b$ $\chi(\boldsymbol{x}) < 0$, the Gaussian curvature is negative at the contact point $\boldsymbol{\xi}_1$, which now lies on the outer sheet of $\mathcal{S}$. The wave singularity corresponding to such a point has the form

$$\frac{A(\hat{\boldsymbol{x}})\hat{\boldsymbol{e}}_{1,2}\hat{\boldsymbol{e}}_{1,2}^T}{|K|^{\frac{1}{2}}(\boldsymbol{\xi}_1)|\boldsymbol{x}|}\,\frac{-1}{\pi(t-t_1)}, \tag{6.4}$$

the Hilbert transform of that in (6.3). See Burridge (1967). Notice that for these values of θ this is the first of the two 'geometrical' wave arrivals and it carries a two-sided singularity. Hence the field must already be non-zero. Indeed, when $\chi(\boldsymbol{x}) < 0$ a weak step singularity arising from small integration loops encircling the conical point arrives first, the associated wavefront being the disk spanning a contact circle $\mathcal{C}_{\mathcal{W}}$ on $\mathcal{W}$. See Burridge (1967) for a treatment of the analogous arrival for cubic elastic media when $\boldsymbol{x}$ is not too near the cone Σ_{++}. For θ near θ_a the stationary point $\boldsymbol{\xi}_1$ is close to the conical point $\boldsymbol{c}_{\mathcal{S}}$. This raises the question of the uniform analytical treatment of the neighborhood of the circle $\mathcal{C}_{\mathcal{W}}$, the boundary of the disk. The analysis of this approximation is not known to the present authors for the time-dependent problem, but Borovikov (2000) has recently given a treatment for the time-harmonic case, and the time-dependent approximation may be derived from this by a Fourier transform, but as far as the authors are aware this has not yet been carried out.

As θ increases from θ_a to θ_c, the stationary point $\boldsymbol{\xi}_1(\theta)$ moves away from the conical point on $\mathcal{S}$ toward the circle $\mathcal{C}_{\mathcal{S}}$ at the lower of $\boldsymbol{\xi}_1(\theta_c) = \boldsymbol{\xi}_1(\theta_c)$, and at the same time the stationary point $\boldsymbol{\xi}_2(\theta)$ moves from $\boldsymbol{\xi}_2(\theta_a)$ outside of the cone Σ_{++} toward the rim of the disk nearest to the 3-axis at the upper point $\boldsymbol{\xi}_1(\theta_c) = \boldsymbol{\xi}_1(\theta_c)$. Both geometrical arrivals come in together at $t = t_1 = t_2$. The direction of $\boldsymbol{x}$ now becomes bi-radial and passes through the conical point $\boldsymbol{c}_{\mathcal{W}}$ on $\mathcal{W}$. Then all the points of $\mathcal{C}_{\mathcal{S}}$ become stationary points and to find the singularities for directions near bi-radial one needs to perform the appropriate uniform asymptotic analysis.

To track these points as θ passes from θ_c to θ_b and to keep the order of arrival times so that $t_1 \le t_2$ the labeling of points must change so that $\boldsymbol{\xi}_1$ becomes $\boldsymbol{\xi}_2$ and vice versa. The old $\boldsymbol{\xi}_2$, renamed as $\boldsymbol{\xi}_1$, now proceeds from the rim to the conical point $\boldsymbol{\xi}_c$ while the old $\boldsymbol{\xi}_1$, renamed as $\boldsymbol{\xi}_2$, proceeds beyond the rim towards the 1-axis, reaching an intermediate position $\boldsymbol{\xi}_2(\theta_b)$ while $\boldsymbol{\xi}_1(\theta_b)$ moves to $\boldsymbol{\xi}_c$.

For θ passing from θ_b to $\pi/2$, $\boldsymbol{\xi}_1$ proceeds on the inner sheet of $\mathcal{S}$ from $\boldsymbol{\xi}_c$ to the direction of the 1-axis and $\boldsymbol{\xi}_2$ also tends to the 1-direction on the outer sheet. In Figure 5 is shown the 13-section of $\mathcal{S}$ with the points $\boldsymbol{\xi}_{1,2}(\theta_{a,b,c})$ indicated. Pairs $\boldsymbol{\xi}_{1,2}$ corresponding to the same θ have parallel normals in the direction of $\boldsymbol{\xi}(\theta)$, making an angle θ with the 3-axis, and indicated as dashed lines in the figure.

6.1 Numerical values of the $G_{ij}(\boldsymbol{x}, t)$ for various $\boldsymbol{x}$ in the 13-plane.

Since the solution is self-similar (homogeneous of degree -2 in $\boldsymbol{x}$ and t) the computation of G was carried out as described above by taking $\boldsymbol{x} = (\sin\theta, 0, \cos\theta)$, for which $|\boldsymbol{x}| = 1$. In Figures 11 - 12 the components of G are plotted as functions of t for each $\boldsymbol{x}$ corresponding to the values of θ listed above. Let us relate these plots to the geometry of the integration loops. Consider, for instance, the plots in these figures for $\theta = 20°$. The corresponding integration loops are shown superimposed on the quarter of $\mathcal{S}$ for which $x_1 > 0$ and $x_3 > 0$ in Figure 6.

Here θ is near θ_a so the $\boldsymbol{x}$ is near $\mathcal{C}_{\mathcal{W}}$ and the inner stationary point marked '$\circledast$' lies near the conical point. Loops are shown for representative values of t. For $\theta = \theta_a$ and t such that the plane $\boldsymbol{\xi}\cdot\boldsymbol{x} = t$ passes through the conical point, the loop corresponding to that time has a cusp at the conical point. The loop near the outer stationary point has the form typical for stationary points with positive Gaussian curvature.

It is clear from the coordinate lines marked on $\mathcal{S}$ that the polarization for the first singularity (on the inner sheet) is in the tensor component transverse to $\boldsymbol{x}$ and lying in the tensorial 'direction'

$$\begin{pmatrix} 0 & 0 & 0 \\ 0 & 1 & 0 \\ 0 & 0 & 0 \end{pmatrix}, \tag{6.5}$$

while the later arrival associated with the outer sheet is in the 'direction'

$$\begin{pmatrix} \cos^2\theta & 0 & -\sin\theta\cos\theta \\ 0 & 0 & 0 \\ -\sin\theta\cos\theta & 0 & \sin^2\theta \end{pmatrix}. \tag{6.6}$$

We can also approximately read off the amplitude since that is inversely proportional to the square root of the Gaussian curvature of $\mathcal{S}$ at the corresponding stationary point. Notice particularly that the curvature goes to infinity at the conical point, leading to zero amplitude there (but indicating that the waveform actually has a different singularity type). On the other hand the curvature goes to zero at points of $\mathcal{C}_{\mathcal{W}}$ where the four special tangent planes $\Pi_{\mathcal{S}}$ touch $\mathcal{S}$.

The details of the loops for an $\boldsymbol{x}$ just outside the cone Σ_{++} are shown in Figure 7. Notice particularly the stationary point marked '$\circledast$', which lies on the inner sheet of $\mathcal{S}$ (as do the other smaller closed loops). The conical point itself is where the loops cross below $\circledast$. The open larger loops belong to the outer sheet of $\mathcal{S}$. The time sequence is such that the outer closed loops are paired with the lower open loops at earlier times and a full intersection of $\boldsymbol{\xi}\cdot\boldsymbol{x} = t$ with $\mathcal{S}$ consists of such pairs of loops until the upper $\circledast$ is reached, when the small closed loops disappear.

The details of the loops for an $\boldsymbol{x}$ just inside the cone Σ_{++} are shown in Figure 8. Now the stationary point marked '$\circledast$' lies on the outer sheet of $\mathcal{S}$. The conical point itself is where the small closed loops (on the inner sheet of $\mathcal{S}$) converge to a point and then open up as closed loops on the outer sheet. The open larger loops belong to the outer sheet of $\mathcal{S}$. The time sequence is that the outer closed loops and the lower open loops are paired at earlier

times, and a full intersection of $\boldsymbol{\xi}\cdot\boldsymbol{x} = t$ with $\mathcal{S}$ consists of two loops until $\circledast$ is reached, when the small closed loops merge with the larger loops to form one large loop like the uppermost (and latest) of the open loops shown.

In Figure 9 we show the loop configuration for an $\boldsymbol{x}$ near the bi-radial direction. There are two stationary points indicated again by '$\circledast$', one just outside the circle $\mathcal{C}_{\mathcal{S}}$ and one just inside. Notice particularly the configuration of the loops near these points.

In Figure 10 we show a similar loop configuration for an $\boldsymbol{x}$ just the other side of the bi-radial direction. Again there are two stationary points indicated by '$\circledast$', one just inside the circle $\mathcal{C}_{\mathcal{S}}$ and one just outside. Notice that the configuration of the loops near these points is similar to the one in Figure 9 but rotated by 180°.

In Figures 11 - 12 are plotted the components of G which are not identically zero by symmetry in the plane $x_2 = 0$. In these figures the $G_{ij}[\boldsymbol{x}(\theta), t]$ are plotted as functions of t for the fixed values of θ indicated on the left vertical scale. The two curves cutting across these indicate the arrival times $t_1(\theta)$ and $t_2(\theta)$. Where these (almost) meet corresponds to θ_c where $t_1 = t_2$. The plot of each G_{ij} starts at the time $t_3(\theta)$ of the conical-point arrival. Notice that only in the range $\theta_a < \theta < \theta_b$ (approximately $25° < \theta < 75°$) is the signal non-zero for $t_3 < t < t_1$. In the same range the arrival at t_1 has the Hilbert transform pulse shape.

The components of G represented in Figures 11 - 12 have δ-like singularities, and so it is difficult to represent their amplitudes in relation to the smooth parts of the signal, the amplitudes of the numerical δ's being inversely proportional to the time step and therefore large and dependent upon the discretization. To give a better representation of the smooth field together with the singularities we have plotted in Figures 13 - 14 the step response obtained from the integrals in (3.28) before differentiation with respect to t, plus the time integral of the third term.

7 Conclusions

We have developed the fundamental solution for the time-dependent system of crystal optics using the Herglotz-Petrovskii formula. This technique represents the solution as integrals around real loops, the intersection of a moving plane $\boldsymbol{\xi}\cdot\boldsymbol{x} = t$ with the slowness surface $\mathcal{S}$, together with a non-propagating term, which is calculated separately. Because of the identities stemming from the residue calculation of Section 3 and other similar relationships it is possible to express the result in terms of Abelian integrals on non-real cycles (Petrovskii, 1945), and possibly a more efficient computation would ensue. These are closely related to the integrals arising in the Cagniard - De Hoop method. See for instance Van der Hijden (1987) for the extension to waves in layered anisotropic elastic media. We have not concerned ourselves with the efficiency of computation, but have used this strikingly geometrical representation to motivate our calculation and to illustrate some special regions of the field, namely the field near the cone of internal conical refraction, and the field near the bi-radial directions. We found that this representation is easily programmable in Matlab.

We have graphically displayed the geometrical entities that come into play and plotted

the signal $G(\boldsymbol{x}, t)$ as functions of t for linear 'gathers' of positions $\boldsymbol{x}$ in the style used in seismic exploration. Since it is not straightforward to represent graphically the amplitude of the Dirac δ we have in one or two places plotted the step response. It is an easy matter to calculate the field to any degree of accuracy in any region using our method. The same method may be used for the fundamental solution for infinitesimal anisotropic elasticity.

We have left for future study the analysis of the uniform asymptotics for field points near the bi-radial directions associated with the conical points $\boldsymbol{c}_{\mathcal{W}}$ on the wave-surface $\mathcal{W}$ and near (the surface of) the cones of internal conical refraction $\Sigma_{\pm}$. We note that Borovikov (2000) has obtained related time-harmonic results where the cone is strictly conical in that it has straight generators but with a nonlinear phase function.

We plan to apply the same method to develop the fundamental solution for the time-dependent system of anisotropic elasticity in the future.

Acknowledgement

The authors are grateful to the Director and staff of the Institute for Mathematics and its Applications, University of Minnesota, where this work was initiated, for providing such excellent research facilities and working environment.

References

1. Atiyah, M.F., R. Bott, and L. Garding, Lacunas for hyperbolic differential operators with constant coefficients I & II, *Acta Mathematica,* **124** (1970), 109-189, and *Acta Mathematica,* **131** (1973), 145-205.

2. Berry, M. V., Conical diffraction asymptotics: fine structure of Poggendorf rings and axial spike. *J. Opt. A: Pure Appl. Opt.* **6** (2004), 289-300.

3. Born, M. and E. Wolf, *Principles of Optics*, Sixth (Corrected) Edition, Pergamon Press, New York, (1989).

4. Borovikov, V.A., The Stationary Phase Method for Surfaces with Conical Points, *Russ. J. Math. Phys.* **7** (2000), 147.

5. Braam, P. J. and Duistermaat, J. J., Normal forms of real symmetric systems with multiplicity, *Indag. Mathem., N.S.* **4** (1993), 407-421.

6. Burridge, R., The singularities on the plane lids of the wave surface of elastic media with cubic symmetry, *Quart. J. Mech. and App. Math.* **XX** (1967), 41-55.

7. Burridge, R., Asymptotic evaluation of integrals related to time-dependent fields near caustics, *SIAM J. App. Math.* **55** (1995), 390-409.

8. Courant, R. and D. Hilbert, *Methods of Mathematical Physics, Vol. II*, Interscience, New York, (1962).

9. Every, A.G., Ballistic phonons and the shape of the ray surface in cubic crystals, *Phys. Rev. B* **24** (1981), 3456-3467.

10. Gel'fand, I.M. and G.E. Shilov, *Generalized Functions, Vol. I*, Academic Press, (1964).

11. Van der Hijden, J.M.T., *Propagation of Transient Elastic Waves in Stratified Anisotropic Media*, North-Holland, Amsterdam, (1987).

12. Hörmander, L., *The Analysis of Linear Partial Differential Operators (II)*, Springer-Verlag, Berlin, (1990).

13. John, F., *Plane Waves and Spherical Means*, Interscience, New York, (1955).

14. Ludwig, D., Conical refraction in crystal optics and hydromagnetics, *Commun. Pure Appl. Math.* **14** (1961), 113.

15. Melrose, R. B. and Uhlmann, G. A., Microlocal structure of involutive conical refraction, *Duke Math. J.* **46** (1979), 571.

16. Moskvin, D.N., V.P. Romanov and A.Y. Val'kov, *Phys. Rev. E* **48** (1993), 1436.

17. M.J.P. Musgrave, *Crystal Acoustics*, Holden-Day, San Francisco, (1970).

18. Osher S. J. and R. P. Fedkiw, *The level set method and dynamic implicit surfaces*, Springer-Verlag, New York, (2002).

19. Petrovskii, I.G., On the diffusion of waves and lacunas for hyperbolic equations, *Mat. Sbornik* **17** (1945), 289-370.

20. Salmon, G., *Analytical geometry of Three Dimensions*, Revised by R.A.P. Rogers, Vol. 2, Longmans, Green & Co., (1915).

21. Shuvalov, A.L. and A.G. Every, Curvature of acoustic slowness surface of anisotropic solids near symmetry axes, *Phys. Rev.* **B53** (1996), 14906.

22. Smit, D. and M.V. de Hoop, The geometry of the hyperbolic system for an anisotropic perfectly elastic medium, *Comm. Math. Phys.* **167** (1995) 255-300.

23. Taylor, M., *Pseudodifferential operators*, Princeton University Press, Princeton, New Jersey, (1981).

24. Uhlmann, G. A., Light intensity distribution in conical refraction, *Commun. Pure Appl. Math.* **35** (1982), 69.

25. Warnick, K.F. and D.V. Arnold, Secondary dark rings of internal conical refraction, *Phys. Rev. E* **55** (1997), 6092-6096.

Appendix A: The cones of internal conical refraction

Here we will derive equation (2.29) for the cones of internal conical refraction. For easy reference we repeat the equation here

$$\chi_{\pm}(\boldsymbol{\xi}) \equiv (\xi_{c3}x_1 \pm \xi_{c1}x_3)\Big(\frac{\xi_{c3}x_1}{\sigma_1} \pm \frac{\xi_{c1}x_3}{\sigma_3}\Big) + x_2^2 = 0. \tag{A.1}$$

Let us first indicate why the planes of multiple tangency $\Pi_{\mathcal{W}}$ to the wave surface $\mathcal{W}$, and dual to the conical points $\boldsymbol{\xi}_c$ on $\mathcal{S}$, touch the wave surface in circles. First we notice that the existence of the conical points $\boldsymbol{\xi}_c$ and the fact that $\mathcal{W}$ is of the fourth degree show that the tangency is along a repeated conic. But the fourth-degree terms in the quartic equation of the wave front $\mathcal{W}$ are $(x_1^2+x_2^2+x_3^2)(x_1^2/\sigma_1+x_2^2/\sigma_2+x_3^2/\sigma_3)$. After a rotation of coordinates so that the the new 3-axis is normal to the plane of tangency, and on setting the new coordinate $x_3' = 1/\sqrt{\sigma_2}$ for the plane of tangency, we find that the equation for the curve of tangency is $\Phi^2 = 0$, where Φ is a quadratic expression in x_1' and x_2' whose second-degree part is a constant multiple of $x_1'^2 + x_2'^2$ and hence represents one of the circles on $\mathcal{W}$ which we have called $\mathcal{C}_{\mathcal{W}}$.

The two double cones of internal conical refraction are the cones with origin O as vertex and passing through the circles $\mathcal{C}_{\mathcal{W}}$, or alternatively the cones of normals to $\mathcal{S}$ at the conical points $\boldsymbol{\xi}_c$. Recall for reference that the plane $x_2 = 0$ cuts $\mathcal{S}$ and $\mathcal{W}$ each in an intersecting circle and ellipse, $\mathcal{S}$ in $\xi_1^2 + \xi_3^2 = \sigma_2$ and $\xi_1^2/\sigma_3 + \xi_3^2/\sigma_1 = 1$, and $\mathcal{W}$ in $x_1^2 + x_3^2 = 1/\sigma_2$ and $\sigma_3 x_1^2/ + \sigma_1 x_3^2 = 1$.

Since (A.1) is homogeneous of degree 2 in (x_1, x_2, x_3), it will be true for any $\boldsymbol{x}$ on the double cones with origin as vertex and passing through a circle $\mathcal{C}_{\mathcal{W}}$ if it is satisfied for all $\boldsymbol{x}$ on $\mathcal{C}_{\mathcal{W}}$. So, first consider a general point $\boldsymbol{x}$ on the circle $\mathcal{C}_{\mathcal{W}}$. For definiteness we assume $\mathcal{C}_{\mathcal{W}}$ to lie in the first quadrant $x_1 > 0$, $x_3 > 0$, in which case the negative signs should be taken in (A.1) as also for the third quadrant. The positive signs should be taken for the second and fourth quadrants.

Draw the chord through $\boldsymbol{x}$ perpendicular to the diameter on which $x_2 = 0$. It is bisected by this diameter at the point $\boldsymbol{x}' = (x_1, 0, x_3)$, say, and each half is of length x_2. Let $\boldsymbol{s}$ be the extremity of the diameter where it touches the circle $x_1^2 + x_3^2 = 1/\sigma_2$ and $\boldsymbol{t}$ be the other extremity where it touches the ellipse $\sigma_3 x_1^2 + \sigma_1 x_3^2 = 1$. Then, from an elementary theorem on intersecting chords of a circle, we know that

$$|\boldsymbol{s} - \boldsymbol{x}'||\boldsymbol{t} - \boldsymbol{x}'| = y^2. \tag{A.2}$$

We shall show that $(\xi_{c3}x_1 - \xi_{c1}x_3)$ is a (positive) scalar multiple of $|\boldsymbol{s} - \boldsymbol{x}|$, and that $-(\xi_{c3}x_1/\sigma_1 - \xi_{c1}x_3/\sigma_3)$ is a (positive) scalar multiple of $|\boldsymbol{t} - \boldsymbol{x}|$, the scalar multiples being the reciprocals $\sqrt{\sigma_2}$ and $1/\sqrt{\sigma_2}$.

First notice that $\boldsymbol{s}$ is normal to the circle $\xi_1^2 + \xi_3^2 = \sigma_2$, $\xi_2 = 0$ at the conical point $\boldsymbol{\xi}_c$ on $\mathcal{S}$, and so

$$\boldsymbol{s} = \boldsymbol{\xi}_c/\sigma_2, \tag{A.3}$$

since $|\boldsymbol{\xi}_c| = \sqrt{\sigma_2}$ and $|\boldsymbol{s}| = 1/\sqrt{\sigma_2}$. Similarly, $\boldsymbol{t}$ is a normal to the ellipse $\xi_1^2/\sigma_3 + \xi_3^2/\sigma_1 = 1$, $\xi_2 = 0$ at the same conical point $\boldsymbol{\xi}_c$, and so it is a multiple of $(\xi_{c1}/\sigma_3, 0, \xi_{c3}/\sigma_1)$. But it lies

on the ellipse $\sigma_3 t_1^2 + \sigma_1 t_3^2 = 1$, and if we take the scalar multiplier to be 1 we easily verify that

$$\begin{aligned} \sigma_3 t_1^2 + \sigma_1 t_3^2 &= \sigma_3(\xi_{c1}/\sigma_3)^2 + \sigma_1(\xi_{c3}/\sigma_1)^2 \\ &= \xi_{c1}^2/\sigma_3 + \xi_{c3}^2/\sigma_1 \\ &= 1. \end{aligned} \tag{A.4}$$

Thus we find that

$$\boldsymbol{t} = (\xi_{c1}/\sigma_3, 0, \xi_{c3}/\sigma_1) \tag{A.5}$$

precisely.

We may express $|\boldsymbol{s} - \boldsymbol{x}'|$ and $|\boldsymbol{t} - \boldsymbol{x}'|$ as twice the areas of the triangles $O\boldsymbol{s}\boldsymbol{x}'$ and $O\boldsymbol{t}\boldsymbol{x}'$ divided by the perpendicular distance $1/\sqrt{\sigma_2}$ from O to the line containing $\boldsymbol{s}$, $\boldsymbol{x}'$, $\boldsymbol{t}$. Twice the area of triangle $O\boldsymbol{s}\boldsymbol{x}'$ is $s_3 x_1 - s_1 x_3$, and so

$$|\boldsymbol{s} - \boldsymbol{x}'| = \sqrt{\sigma_2}(s_3 x_1 - s_1 x_3) = \frac{\xi_{c3} x_1 - \xi_{c1} x_3}{\sqrt{\sigma_2}} \tag{A.6}$$

and twice the area of triangle $O\boldsymbol{t}\boldsymbol{x}'$ is $-(t_3 x_1 - t_1 x_3)$, and so

$$|\boldsymbol{t} - \boldsymbol{x}'| = -\sqrt{\sigma_2}(t_3 x_1 - t_1 x_3) = -\sqrt{\sigma_2}\Big(\frac{\xi_{c3} x_1}{\sigma_1} - \frac{\xi_{c1} x_3}{\sigma_3}\Big) \tag{A.7}$$

On using (A.6) and (A.7) in (A.2) we obtain (A.1) with negative signs as required. Then by taking the circle $\mathcal{C}_{\mathcal{W}}$ to lie in the second or fourth quadrants we account for the positive signs in (A.1).

Appendix B: The integrals $I^{(0)}$, $I^{(2)}$, $I^{(4)}$ and the static term

As stated in Section 5 we need integrals of the form

$$I^{(0)} = \int_0^{2\pi} \frac{\mathrm{d}\phi}{D}, \quad I^{(2)}_{pq} = \int_0^{2\pi} \frac{x^\perp_p x^\perp_q \,\mathrm{d}\phi}{D^2}, \quad I^{(4)}_{pqrs} = \int_0^{2\pi} \frac{x^\perp_p x^\perp_q x^\perp_r x^\perp_s \,\mathrm{d}\phi}{D^3}, \tag{B.8}$$

where $D = \boldsymbol{x}^{\perp T}\boldsymbol{\sigma}\boldsymbol{x}^\perp$ and the superscript indicates the rank of the tensor. We begin with $I^{(0)}$ from which the others may be derived by means of

$$I^{(2)}_{pq} = -\frac{\partial I^{(0)}}{\partial \sigma_{pq}}, \quad I^{(4)}_{pqrs} = \frac{1}{2}\frac{\partial^2 I^{(0)}}{\partial\sigma_{pq}\partial\sigma_{rs}}. \tag{B.9}$$

Let us further suppose that the triad $\hat{\boldsymbol{x}}$, $\hat{\boldsymbol{y}}$, $\hat{\boldsymbol{z}}$ is chosen so that $\hat{\boldsymbol{y}}$ and $\hat{\boldsymbol{z}}$ are principal axes of the section of the ellipsoid $\boldsymbol{\xi}^T\boldsymbol{\sigma}^{-1}\boldsymbol{\xi} = 1$ by the plane $\boldsymbol{\xi}\cdot\boldsymbol{x} = 0$. Then

$$\begin{aligned} I^{(0)} &= \int_0^{2\pi} \frac{\mathrm{d}\phi}{D} \\ &= \int_0^{2\pi} \frac{\mathrm{d}\phi}{a\cos^2\phi + b\sin^2\phi} \\ &= 4\int_0^{\pi} \frac{\mathrm{d}\phi}{a(1+\cos 2\phi) + b(1-\cos 2\phi)} \\ &= 2\int_0^{2\pi} \frac{\mathrm{d}\psi}{(a+b) + (a-b)\cos\psi}, \end{aligned} \tag{B.10}$$

where $a = \hat{\boldsymbol{y}}^T\boldsymbol{\sigma}\hat{\boldsymbol{y}}$, $b = \hat{\boldsymbol{z}}^T\boldsymbol{\sigma}\hat{\boldsymbol{z}}$, and we have changed integration variable to $\psi = 2\phi$. Setting, in the usual way, $z = \mathrm{e}^{\mathrm{i}\psi}$, $\mathrm{d}\psi = \mathrm{d}z/\mathrm{i}z$, we obtain

$$\begin{aligned} I^{(0)} &= -2\mathrm{i}\oint_{|z|=1} \frac{\mathrm{d}z}{\frac{1}{2}(a-b)z^2 + (a+b)z + \frac{1}{2}(a-b))} \\ &= -\frac{4\,\mathrm{i}}{(a-b)}\oint_{|z|=1} \frac{\mathrm{d}z}{(z+\alpha)(z+\beta)}, \end{aligned} \tag{B.11}$$

where

$$\alpha + \beta = \frac{2(a+b)}{a-b}, \qquad \alpha\beta = 1 \tag{B.12}$$

Evaluating (B.11) by residues at α where $|\alpha| < 1$ we get

$$\begin{aligned} I^{(0)} &= \frac{8\pi}{(a-b)(-\alpha+\beta)} \\ &= -\frac{2\pi}{\sqrt{ab}}, \end{aligned} \tag{B.13}$$

where we have used the obvious identity $(-\alpha+\beta)^2 = (\alpha+\beta)^2 - 4\alpha\beta$. But ab is the determinant of

$$\begin{pmatrix} \hat{\boldsymbol{y}}^T \\ \hat{\boldsymbol{z}}^T \end{pmatrix} \boldsymbol{\sigma} \begin{pmatrix} \hat{\boldsymbol{y}} & \hat{\boldsymbol{z}} \end{pmatrix} \tag{B.14}$$

which is the cofactor of $\hat{\boldsymbol{x}}^T\boldsymbol{\sigma}\hat{\boldsymbol{x}}$ in

$$\det\left\{ \begin{pmatrix} \hat{\boldsymbol{x}}^T \\ \hat{\boldsymbol{y}}^T \\ \hat{\boldsymbol{z}}^T \end{pmatrix} \boldsymbol{\sigma} \begin{pmatrix} \hat{\boldsymbol{x}} & \hat{\boldsymbol{y}} & \hat{\boldsymbol{z}} \end{pmatrix} \right\}, \tag{B.15}$$

i.e. it is the 11 component of

$$\mathrm{adj}\left\{ \begin{pmatrix} \hat{\boldsymbol{x}}^T \\ \hat{\boldsymbol{y}}^T \\ \hat{\boldsymbol{z}}^T \end{pmatrix} \boldsymbol{\sigma} \begin{pmatrix} \hat{\boldsymbol{x}} & \hat{\boldsymbol{y}} & \hat{\boldsymbol{z}} \end{pmatrix} \right\} = \begin{pmatrix} \hat{\boldsymbol{x}}^T \\ \hat{\boldsymbol{y}}^T \\ \hat{\boldsymbol{z}}^T \end{pmatrix} \mathrm{adj}\boldsymbol{\sigma} \begin{pmatrix} \hat{\boldsymbol{x}} & \hat{\boldsymbol{y}} & \hat{\boldsymbol{z}} \end{pmatrix} = F, \text{ say,} \tag{B.16}$$

where we have made use of the fact that the adjoint of a product is the product of the adjoints in the reverse order and that the adjoint of an orthogonal matrix is its transpose. The 3×3 component of this is

$$F = \hat{\boldsymbol{x}}^T \mathrm{adj}\boldsymbol{\sigma}\hat{\boldsymbol{x}}. \tag{B.17}$$

Further, to facilitate differentiation with respect to σ_{jq} we write

$$F = \hat{\boldsymbol{x}}^T \mathrm{adj}\boldsymbol{\sigma}\hat{\boldsymbol{x}} = \tfrac{1}{2} Z_{jk} Z_{qr} \sigma_{jq} \sigma_{kr}, \tag{B.18}$$

where

$$Z_{jk} = \epsilon_{ijk}\hat{x}_i, \tag{B.19}$$

and we are assuming $\boldsymbol{\sigma}^T = \boldsymbol{\sigma}$. Thus writing

$$\frac{\partial F}{\partial \sigma_{kr}} = Z_{jk} Z_{qr} \sigma_{jq}, \quad \frac{\partial^2 F}{\partial \sigma_{kr}\sigma_{jq}} = Z_{jk} Z_{qr}, \tag{B.20}$$

from which we obtain

$$\begin{aligned} I^{(0)} &= \frac{2\pi}{F^{\frac{1}{2}}}, \\ I^{(2)}_{jq} &= \frac{2\pi}{F^{\frac{3}{2}}} (Z^T\boldsymbol{\sigma}Z)_{jq}, \\ I^{(4)}_{jqkr} &= -\frac{2\pi}{F^{\frac{3}{2}}} Z_{jk}Z_{qr} + \frac{3\pi}{2F^{\frac{5}{2}}} (Z^T\boldsymbol{\sigma}Z)_{jq}(Z^T\boldsymbol{\sigma}Z)_{kr}. \end{aligned} \tag{B.21}$$

It is now straightforward to write the integral of (5.5), call it K. Then

$$\begin{aligned} K_{ip} &= \int_0^{2\pi} \frac{\partial^2}{\partial\mu^2}\left(\frac{\hat\xi_i\hat\xi_p^T}{\hat{\boldsymbol\xi}^T\boldsymbol\sigma\hat{\boldsymbol\xi}}\right)\Big|_{\mu=0} \mathrm{d}\phi \\ &= 2\,[I^{(0)}\,\hat x_i\hat x_p^T - (\hat{\boldsymbol x}^T\boldsymbol\sigma\hat{\boldsymbol x})\,I_{ip}^{(2)} - 2(\boldsymbol\sigma\hat{\boldsymbol x})_k(\hat x_i I_{kp}^{(2)} + I_{ik}^{(2)}\hat x_p) + 4(\boldsymbol\sigma\hat x)_k(\boldsymbol\sigma\hat x)_\ell I_{k\ell ip}]. \end{aligned} \tag{B.22}$$

Hence, using (B.21) in (B.22) we get

$$\begin{aligned} K_{ip} &= 2\pi\,\{2F^{-\frac12}\,\hat x_i\hat x_p^T - (\hat{\boldsymbol x}^T\boldsymbol\sigma\hat{\boldsymbol x})\,F^{-\frac32}(Z^T\boldsymbol\sigma Z)_{ip} \\ &\quad -2F^{-\frac32}(\boldsymbol\sigma\hat{\boldsymbol x})_k[\hat x_i(Z^T\boldsymbol\sigma Z)_{kp} + (Z^T\boldsymbol\sigma Z)_{ik}\hat x_p] \\ &\quad -2F^{-\frac32}(\boldsymbol\sigma\hat{\boldsymbol x})_k(\boldsymbol\sigma\hat{\boldsymbol x})_\ell Z_{ki}Z_{\ell p} \\ &\quad +3F^{-\frac52}(\boldsymbol\sigma\hat{\boldsymbol x})_k(\boldsymbol\sigma\hat{\boldsymbol x})_\ell(Z^T\boldsymbol\sigma Z)_{k\ell}(Z^T\boldsymbol\sigma Z)_{ip}\}. \end{aligned} \tag{B.23}$$

Or, in subscript-free notation

$$\begin{aligned} K &= \frac{2\pi}{F^{\frac12}}\left\{2\hat{\boldsymbol x}\hat{\boldsymbol x}^T - \frac{\hat{\boldsymbol x}^T\boldsymbol\sigma\hat{\boldsymbol x}}{F}W - \frac{2}{F}(\hat{\boldsymbol x}\mathbf{w}^TW + W\mathbf{w}\hat{\boldsymbol x}^T)\right. \\ &\quad \left. -\frac{2}{F}Z^T\mathbf{w}\mathbf{w}^TZ + \frac{3}{F^2}(\mathbf{w}^TW\mathbf{w})W\right\}, \end{aligned} \tag{B.24}$$

where we have written

$$\mathbf{w} = \boldsymbol\sigma\hat{\boldsymbol x}, \quad W = Z^T\boldsymbol\sigma Z. \tag{B.25}$$

Thus we may write the static term of (3.28) as

$$\begin{aligned} -\frac{t}{8\pi^2}\int_\Omega \frac{\hat{\boldsymbol\xi}\hat{\boldsymbol\xi}^T}{\hat{\boldsymbol\xi}^T\boldsymbol\sigma\hat{\boldsymbol\xi}}\,\delta''(\hat{\boldsymbol\xi}\cdot\boldsymbol x)\,\mathrm{d}\Omega &= -\frac{t}{4\pi F^{\frac12}|\boldsymbol x|^3}\left\{2\hat{\boldsymbol x}\hat{\boldsymbol x}^T - \frac{\hat{\boldsymbol x}^T\boldsymbol\sigma\hat{\boldsymbol x}}{F}W\right. \\ &\quad -\frac{2}{F}(\boldsymbol h\mathbf{w}^TW + W\mathbf{w}\hat{\boldsymbol x}^T) \\ &\quad \left. -\frac{2}{F}Z^T\mathbf{w}\mathbf{w}^TZ + \frac{3}{F^2}(\mathbf{w}^TW\mathbf{w})W\right\}, \end{aligned} \tag{B.26}$$

with $\mathbf{w}$ and W given by (B.25), and F and Z by (B.18) and (B.19).

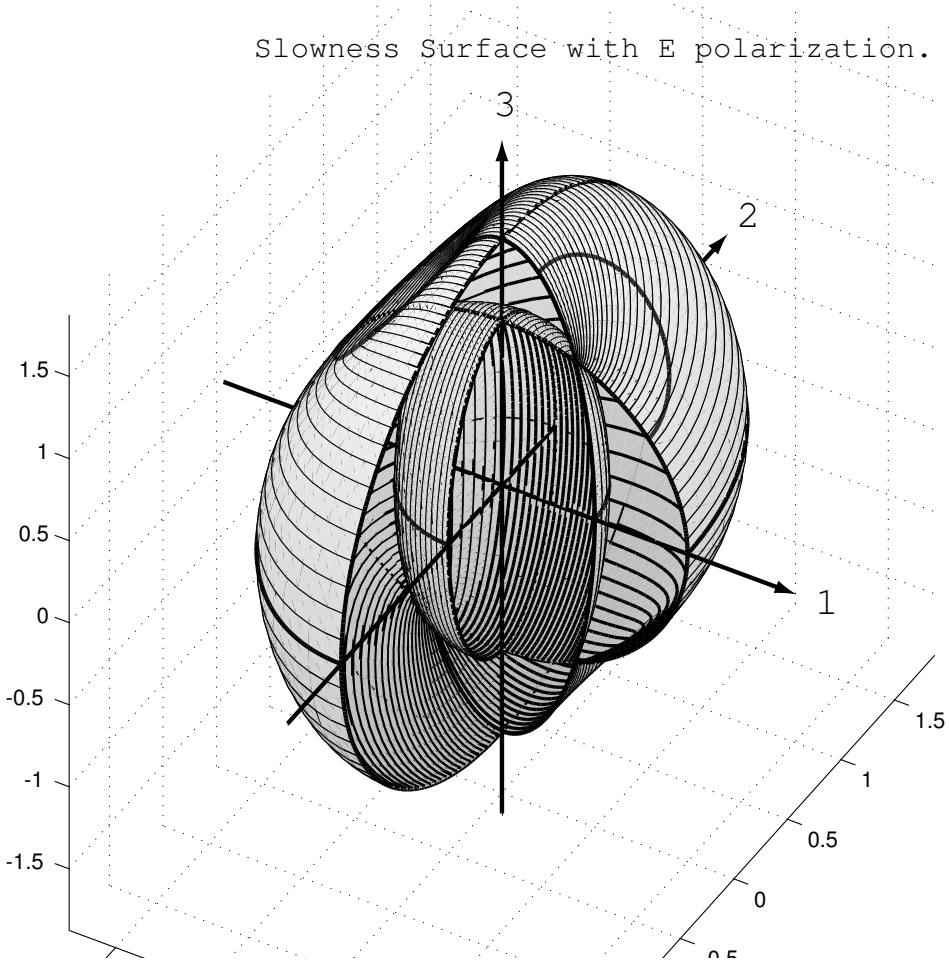

Figure 1: This shows the slowness surface $\mathcal{S}$ cut away to reveal the inner sheet. The contours drawn on the surface are tangent everywhere to the polarization $\boldsymbol{e}$. The thicker contours drawn in each coordinate plane show the circle and ellipse in which that plane cuts the surface. The conical points are clearly visible as the intersections of the ellipse and circle in the (1-3)-plane. There are also four planes each of which touches $\mathcal{S}$ along a circle. The four circles (only half of one being clearly visible) are drawn as heavy lines surrounding the conical points on the outer sheet.

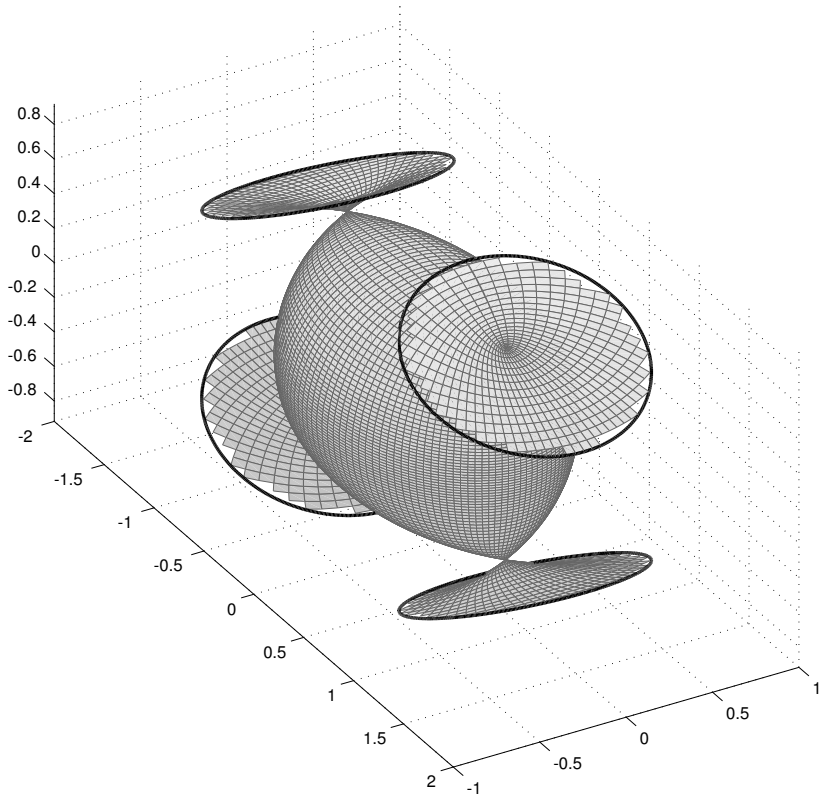

Figure 2: This shows the inner sheet of the wave-surface $\mathcal{W}$ reciprocal to the outer sheet of the slowness surface $\mathcal{S}$. The four prominent 'ears' have negative Gaussian curvature and correspond to four regions with negative curvature on $\mathcal{S}$. The dark circles are the circles of contact $\mathcal{C}_{\mathcal{W}}$ of the four special tangent planes $\Pi_{\mathcal{W}}$. These circles correspond to conical points on $\mathcal{S}$. Reciprocally the conical points of $\mathcal{W}$ shown here correspond to similar circles of tangency on $\mathcal{S}$. This surface joins smoothly onto the outer sheet of $\mathcal{W}$ shown in the next figure along the contact circles. The fundamental solution is weak on the circles $\mathcal{C}_{\mathcal{W}}$, but the strongest part of the field is near the conical points $\boldsymbol{c}_{\mathcal{W}}$ of $\mathcal{W}$.

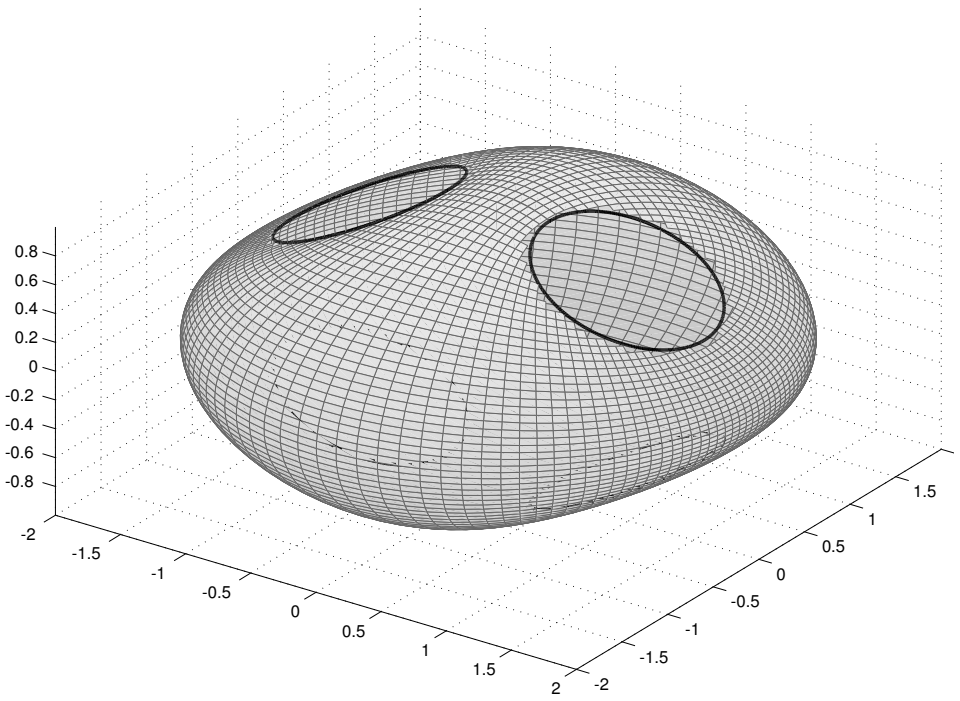

Figure 3: This shows the outer sheet of the wave-surface $\mathcal{W}$ reciprocal to the inner sheet of the slowness surface $\mathcal{S}$. The dark circles are the circles of contact $\mathcal{C}_{\mathcal{W}}$ for the four multiply tangent planes $\Pi_{\mathcal{W}}$. These circles correspond to conical points on $\mathcal{S}$. This surface joins smoothly onto the inner sheet of $\mathcal{W}$ shown in the previous figure along the four circles $\mathcal{C}_{\mathcal{W}}$ where the signal is relatively weak. An additional weak wave singularity (arrival) resides on the disks spanning these circles.

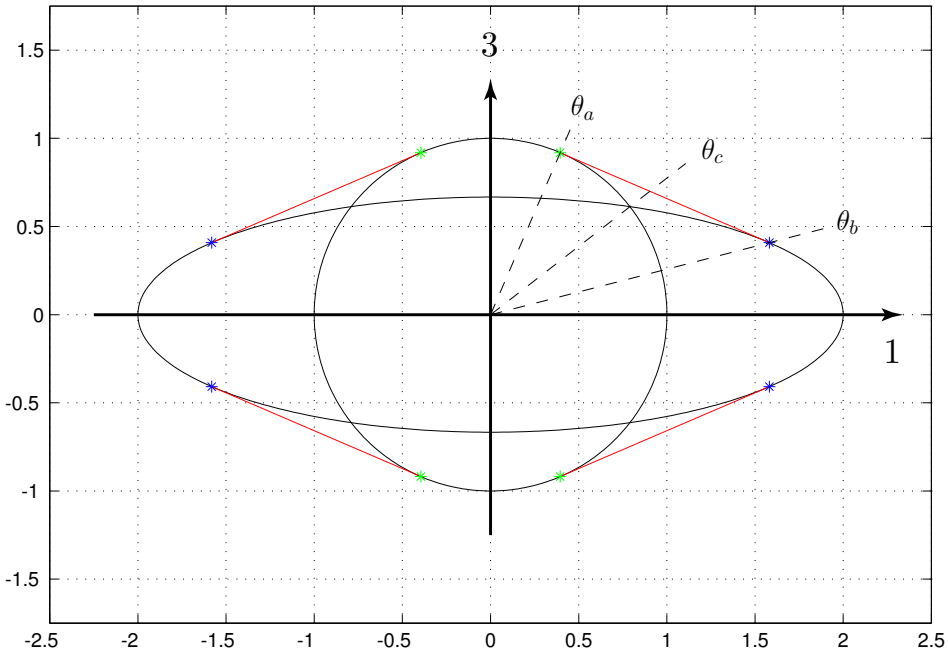

Figure 4: This shows the 13-section of the wave surface $\mathcal{W}$ for fixed time $t = 1$. Notice the ellipse and the circle which intersect at the conical points of $\mathcal{W}$, the bi-radials, making angle θ_c with the 3-axis. The angles θ_a, θ_b, and θ_c, measured from the 3-axis, are indicated. Notice also the segments of common tangents which represent the disks $\mathcal{D}_{\mathcal{W}}$ forming a part of the wavefront carrying a weak singularity.

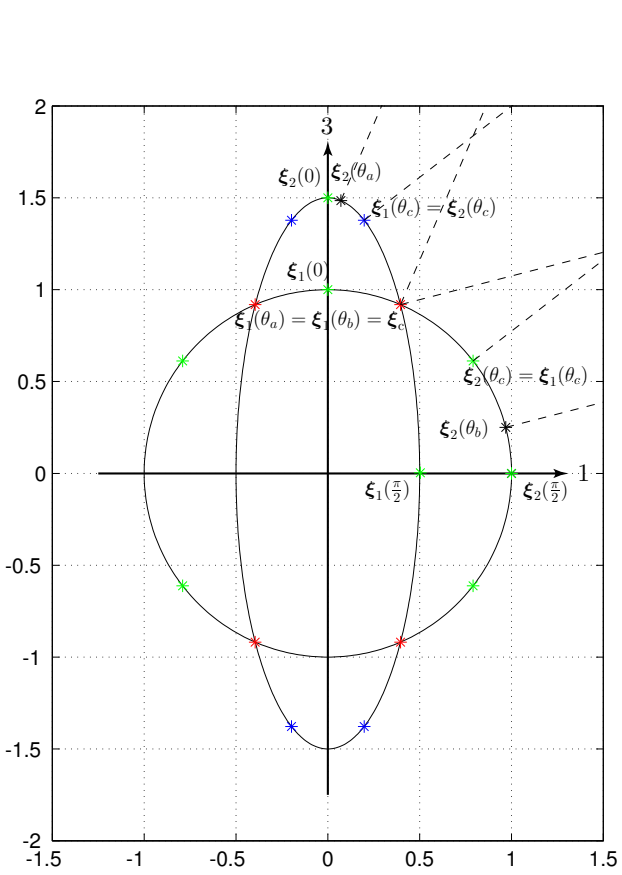

Figure 5: This shows the 13-section of the slowness surface $\mathcal{S}$. Notice the ellipse and the circle which intersect at the conical points of $\mathcal{S}$, the bi normals, making angle θ_c with the 3-axis. The points $\boldsymbol{\xi}_{1,2}(\theta)$ are indicated for $\theta = \theta_a, \theta_b, \theta_c$. Notice also the segments of common tangents which represent the disks $\mathcal{D}_{\mathcal{W}}$ forming a part of the wavefront which carries a weak, early arriving, singularity.

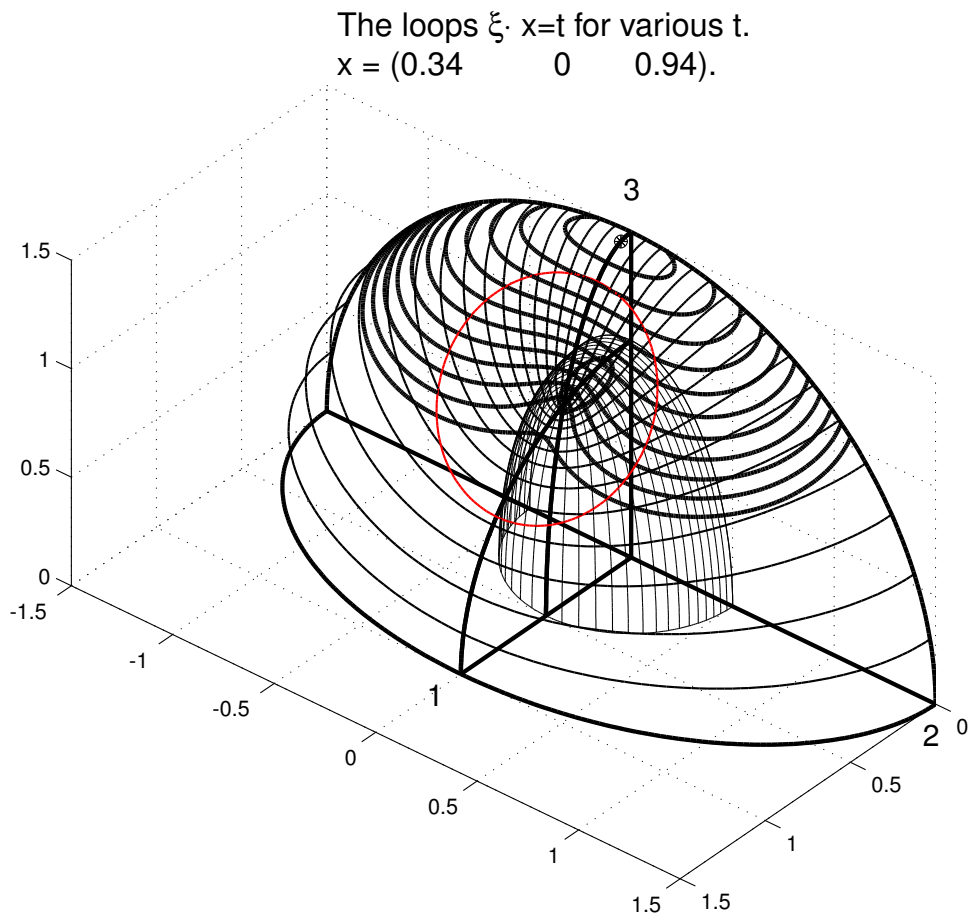

Figure 6: This shows one quarter of $\mathcal{S}$ with integration loops for selected values of t. The points marked '⊛' indicate the points of tangency where first the inner loop and later the outer loop shrink to single points. The wave-field δ-like singularities associated with these points have the polarization indicated by the thinner lines drawn on $\mathcal{S}$.

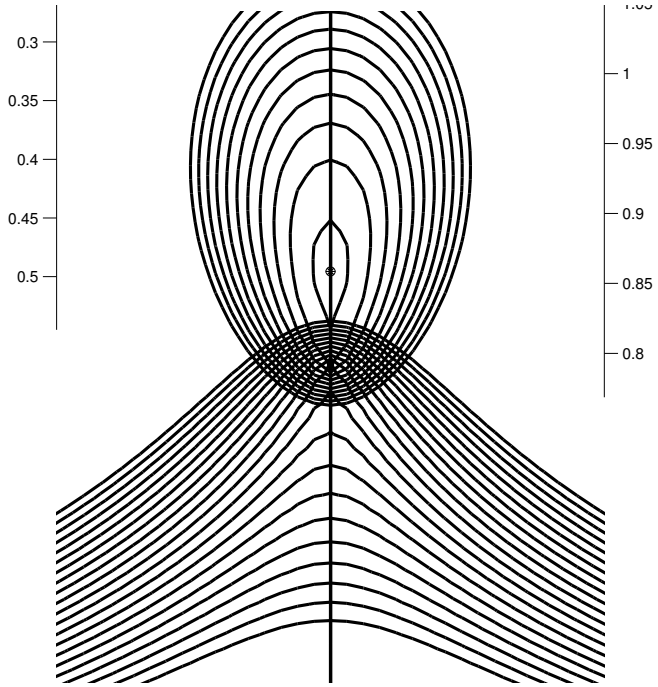

Figure 7: This shows the configuration of loops near the conical point for $\theta = 15°$. Notice the stationary point surrounded by the small loop on the inner sheet of $\mathcal{S}$. The conical point appears where the curves cross. The signal from the conical point is zero in all components. $\chi(\boldsymbol{x}) > 0$ and so $\boldsymbol{x}$ is (just) outside the cone through the circle of tangency $\mathcal{C}_{\mathcal{W}}$ and the singularity at $\circledast$ is δ-like, appropriate to positive curvature.

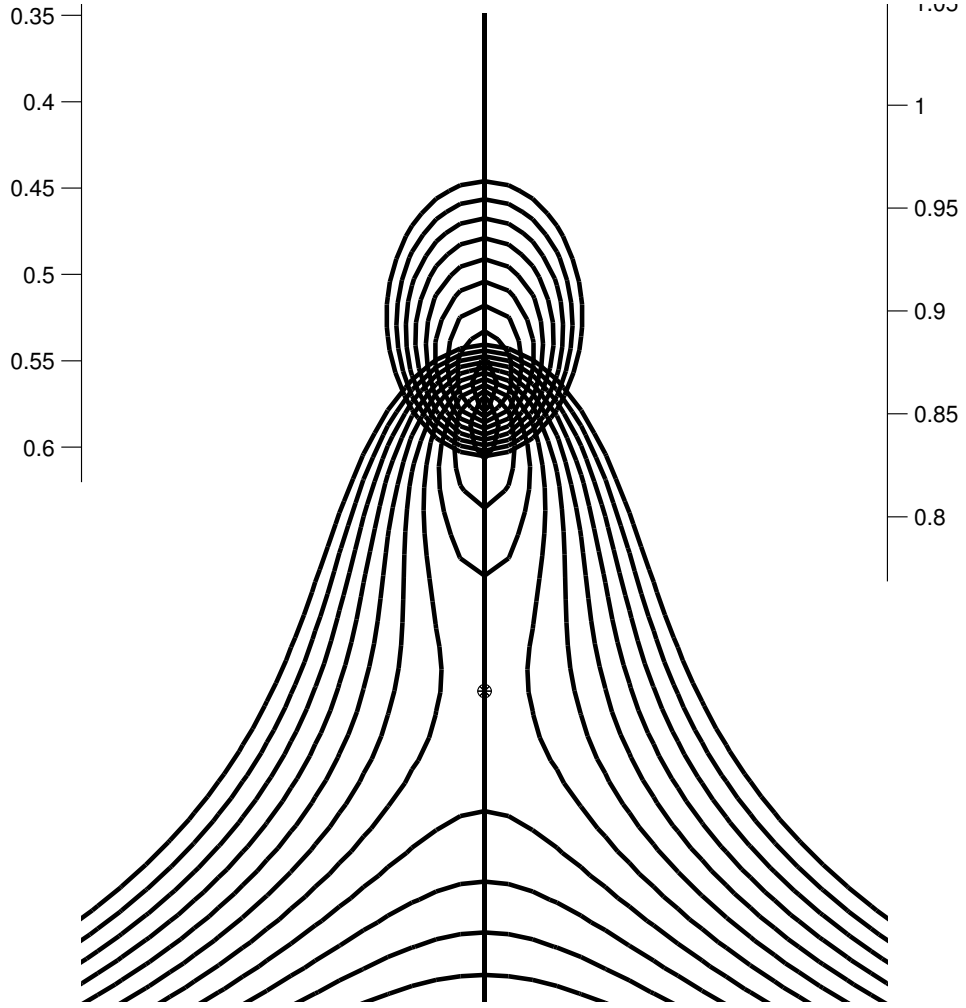

Figure 8: This shows the configuration of loops near the conical point for $\theta = 30°$. Notice the stationary point ⊛ in a neighborhood of negative Gaussian curvature on the outer sheet of $\mathcal{S}$. The local shape of the loops is hyperbolic. The conical point appears where the loops converge above it. $\chi(\boldsymbol{x}) < 0$ here and so $\boldsymbol{x}$ is inside the cone through the circle of tangency $\mathcal{C}_{\mathcal{W}}$ and there is a nonzero step-like arrival when the loops pass over the conical point. As t increases near these small loops surround the conical point on the inner sheet, shrink to the conical point, and then grow around it on the outer sheet.

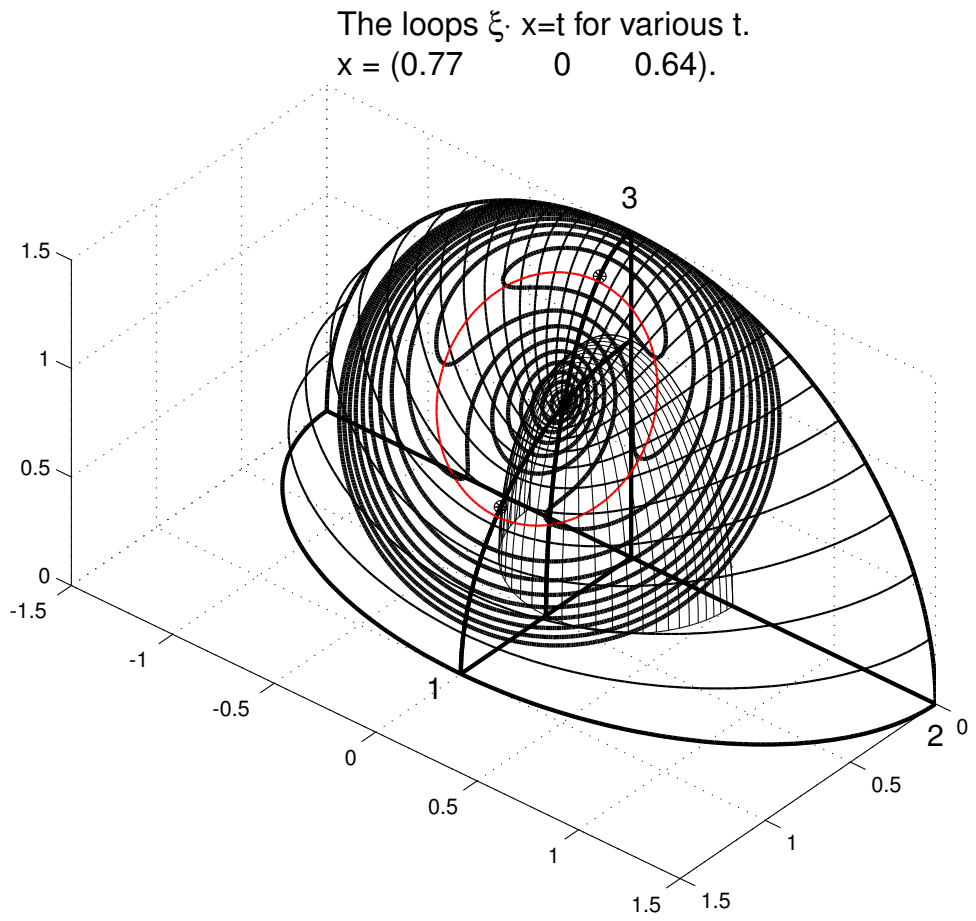

Figure 9: This shows one quarter of $\mathcal{S}$ with integration loops for selected values of t. The stationary points marked '⊛' indicate the points of tangency where first the inner loop and later the outer loop shrink to single points. Notice that the upper stationary point, just outside the circle $\mathcal{C}_{\mathcal{S}}$, is associated with positive curvature while the lower one, just inside the circle $\mathcal{C}_{\mathcal{S}}$, is associated with negative curvature. The wave-field singularities associated with these points have the polarizations indicated by the thinner lines drawn on $\mathcal{S}$. Thus the upper stationary point has polarization in the 13-plane while the lower has polarization in the 2-direction. Notice that the loops near these points remain close to $\mathcal{C}_{\mathcal{S}}$.The types of singularities are appropriate to the sign of the curvature at the '⊛'. (Compare with Figure 10.)

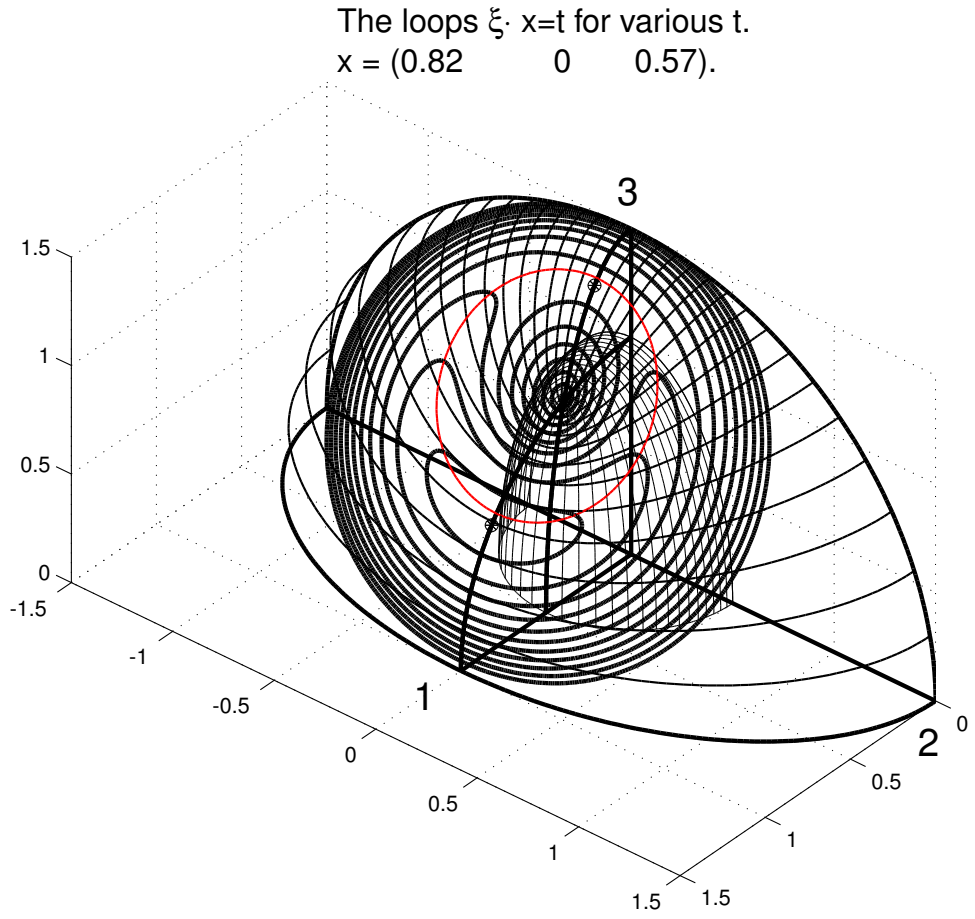

Figure 10: This is similar to Figure 9. Notice that the upper stationary point, just inside the circle $\mathcal{C}_{\mathcal{S}}$, is associated with negative curvature while the lower one, just outside the circle $\mathcal{C}_{\mathcal{S}}$, is associated with positive curvature. The wave-field singularities associated with these points have the polarizations indicated by the thinner lines drawn on $\mathcal{S}$.

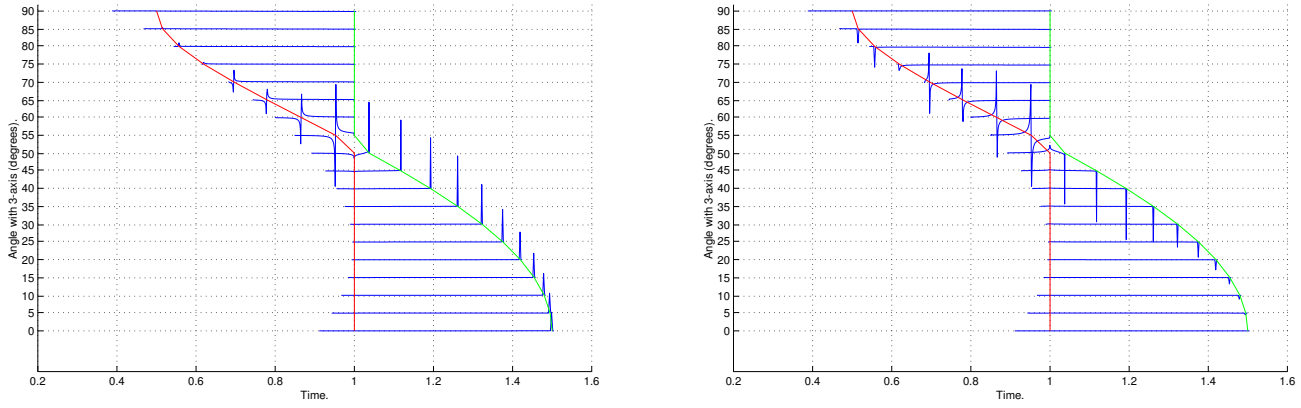

(a) (b)

Figure 11: This plots (a): $G_{11}(\boldsymbol{x},t)$ and (b): $G_{31}(\boldsymbol{x},t)$ for $\boldsymbol{x}$ having the direction $(\sin\theta, 0, \cos\theta)$ for θ increasing by steps of 5° from 0° to 90°. See the text for further details.

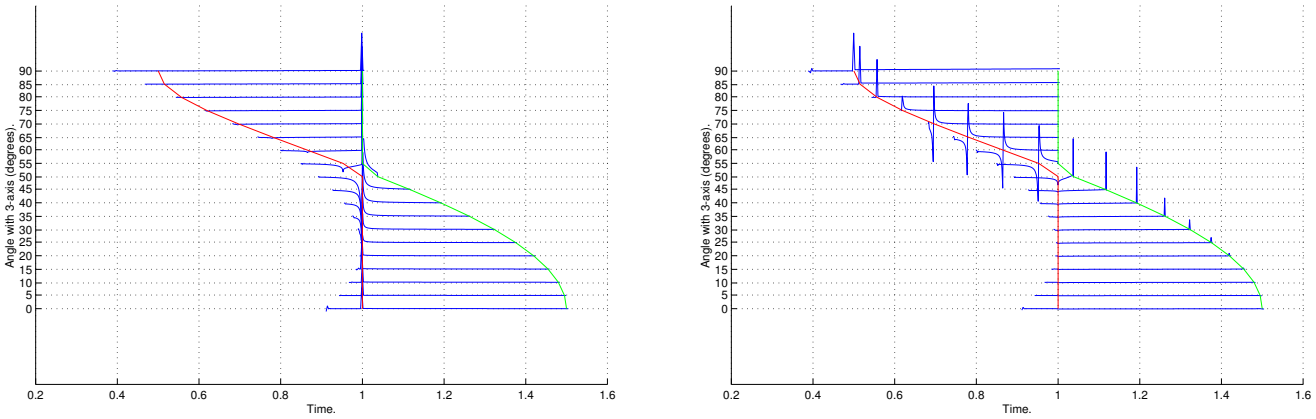

(a) (b)

Figure 12: This plots (a): $G_{22}(\boldsymbol{x},t)$ and (b): $G_{33}(\boldsymbol{x},t)$ for $\boldsymbol{x}$ having the direction $(\sin\theta, 0, \cos\theta)$ for θ increasing by steps of 5° from 0° to 90°. See the text for further details.

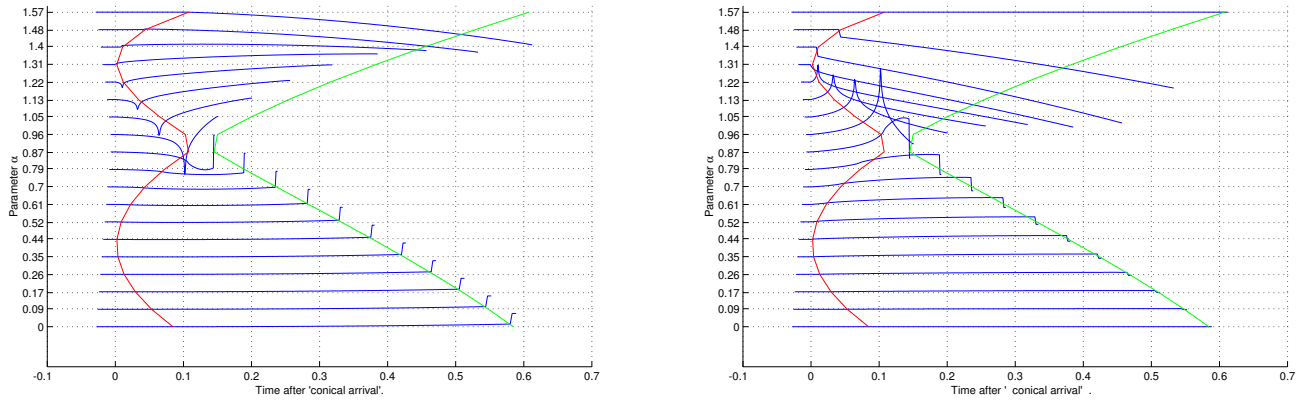

(a) (b)

Figure 13: This plots (a): $WG_{11}(\boldsymbol{x},t)$ and (b): $WG_{31}(\boldsymbol{x},t)$ of the **step response** for $\boldsymbol{x}$ having the direction $(\sin\theta, 0, \cos\theta)$ for θ increasing by steps of 5° from 0° to 90°. See the text for further details.

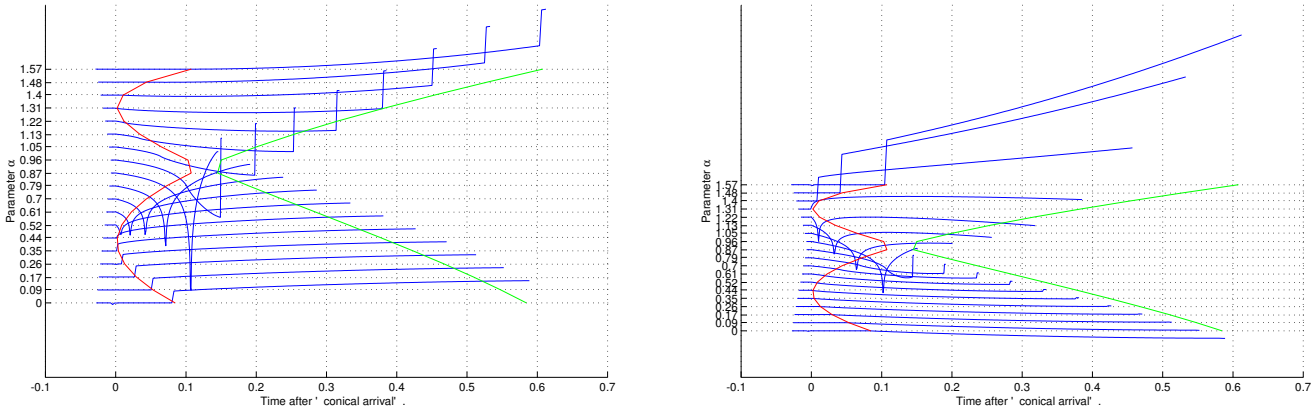

(a) (b)

Figure 14: This plots (a): $WG_{22}(\boldsymbol{x}, t)$ and (b): $WG_{33}(\boldsymbol{x}, t)$ of the **step response** for $\boldsymbol{x}$ having the direction $(\sin\theta, 0, \cos\theta)$ for θ increasing by steps of $5°$ from $0°$ to $90°$. See the text for further details.